Journal of Photonics for Energy

PhotonicsforEnergy.SPIEDigitalLibrary.org

The role of photonics in energy

Zakya H. Kafafi
Raúl J. Martín-Palma
Ana F. Nogueira
Deirdre M. O'Carroll
Jeremy J. Pietron
Ifor D. W. Samuel
Franky So
Nelson Tansu
Loucas Tsakalakos

SPIE.

Downloaded From: http://photonicsforenergy.spiedigitallibrary.org/ on 01/26/2016 Terms of Use: http://spiedigitallibrary.org/ss/TermsOfUse.aspx

REVIEW

The role of photonics in energy

Zakya H. Kafafi,[a,*] Raúl J. Martín-Palma,[b] Ana F. Nogueira,[c] Deirdre M. O'Carroll,[d] Jeremy J. Pietron,[e] Ifor D. W. Samuel,[f] Franky So,[g] Nelson Tansu,[a] and Loucas Tsakalakos[h]

[a]Lehigh University, Center for Photonics and Nanoelectronics, Department of Electrical and Computer Engineering, Bethlehem, Pennsylvania 18015, United States
[b]Universidad Autónoma de Madrid, Departamento de Física Aplicada, Cantoblanco, Madrid 28049, Spain
[c]University of Campinas, Laboratório de Nanotecnologia e Energia Solar, Campinas-SP 13083970, Brazil
[d]Rutgers University, Department of Materials Science and Engineering, Department of Chemistry and Chemical Biology and IAMDN, Piscataway, New Jersey 08854, United States
[e]Surface Chemistry Branch, Code 6170, Naval Research Laboratory, Washington, DC 20375, United States
[f]University of St Andrews, Organic Semiconductor Centre, SUPA, School of Physics and Astronomy, St. Andrews, Fife KY16 9SS, United Kingdom
[g]North Carolina State University, Department of Materials Science and Engineering, Raleigh, North Carolina 27695, United States
[h]General Electric–Global Research Center, Electrical Technologies and Systems, Micro and Nano Structures Technologies, Photonics Laboratory, Niskayuna, New York 12309, United States

Abstract. In celebration of the 2015 International Year of Light, we highlight major breakthroughs in photonics for energy conversion and conservation. The section on energy conversion discusses the role of light in solar light harvesting for electrical and thermal power generation; chemical energy conversion and fuel generation; as well as photonic sensors for energy applications. The section on energy conservation focuses on solid-state lighting, flat-panel displays, and optical communications and interconnects. © *The Authors. Published by SPIE under a Creative Commons Attribution 3.0 Unported License. Distribution or reproduction of this work in whole or in part requires full attribution of the original publication, including its DOI.* [DOI: 10.1117/1.JPE.5.050997]

Keywords: chemical energy conversion; dye sensitized cells; electrical energy conversion; energy; energy conservation; energy conversion; flat panel displays; International Year of Light; light management; light-emitting diodes; optical communications; optical interconnects; optoelectronics; organic light-emitting diodes; organic photovoltaics; organic-inorganic hybrid cells; perovskite solar cells; photocatalysis; photoelectrochemical solar cells; photonic crystals; photonics; photovoltaics; plasmonics; sensors; solar cells; solar fuels; solar harvesting; solid-state lighting; sun-tracking systems; thermal energy conversion; water-splitting.

Paper 15040V received May 9, 2015; accepted for publication Aug. 3, 2015; published online Oct. 12, 2015.

1 Historical Background

The most comprehensive ancient account of the science of light is a millennium old, dating from the Islamic golden age when the Arab scholar Ibn al-Haytham (Alhazen) composed and published his seminal seven-volume *Book on Optics*. It was nearly 700 years later that Christiaan Huygens developed a wave theory of light, while Newton proposed a corpuscular (particle) theory of light.

Authors are listed alphabetically.

*Address all correspondence to: Zakya H. Kafafi, E-mail: kafafiz@gmail.com; Raúl J. Martín-Palma, E-mail: rauljose.martin@uam.es; Ana Flávia Nogueira, E-mail: anaflavia@iqm.unicamp.br; Deirdre M. O'Carroll, E-mail: ocarroll@rci.rutgers.edu; Jeremy J. Pietron, E-mail: jeremy.pietron@nrl.navy.mil; Ifor D. W. Samuel, E-mail: idws@st-andrews.ac.uk; Franky So, E-mail: fso@ncsu.edu; Nelson Tansu, E-mail: tansu@lehigh.edu; and Loucas Tsakalakos, E-mail: tsakalakos@ge.com

Downloaded From: http://photonicsforenergy.spiedigitallibrary.org/ on 01/26/2016 Terms of Use: http://spiedigitallibrary.org/ss/TermsOfUse.aspx

In his book, *A Dynamical Theory of the Electromagnetic Field*, Maxwell mathematically unified light, electricity, and magnetism.[1] This modern theory of light is only 150 years old!

These great milestones were followed by the work of Einstein,[2] who introduced the concept of photons to explain photoelectric effect data in terms of light energy being carried in discrete, quantized packets. He demonstrated that only photons with a certain threshold frequency (energy) impinged upon a metal surface can cause the ejection of electrons. The discovery of the law of this photoelectric effect was a foundation of the quantum revolution and was the primary reason for the Nobel Prize awarded to Einstein in 1922.[3]

A recent and elegant demonstration of light's dual nature was reported by the group of Carbone at École Polytechnique Fédérale de Lausanne (EPFL) in Switzerland, who captured a snapshot of the concurrent behavior of light as both a wave and a stream of particles[4] (Fig. 1).

Understanding the quantum nature of light and electrons was crucial to the discovery of other phenomena that involve the interaction of light with electric charges, such as the photoconductive effect, i.e., photoconductivity, the photovoltaic (PV) effect, and the photoelectrochemical (PEC) effect.

In this paper, we will review some of the enabling photonic technologies that followed based on last century's fundamental discoveries related to the interaction of light and matter. Section 1 gives an overview of the role that photonics plays in power generation through electrical, thermal, and chemical energy conversion, as well as in sensor technology. Section 2 describes technological advances where photonics is important for energy conservation. It covers solid-state lighting, flat-panel displays, and optical communications and interconnects. Advances in photonics such as the development of the worldwide optical communications network that carried the news of Charles Kao's receiving the Nobel Prize in 2009,[5] thanks to his proposal 50 years ago to use optical fibers to transmit phone calls across great distances, will be highlighted. Other examples will include the revolution in solid-state lighting that earned *Isamu Akasaki*, *Hiroshi Amano*, and *Shuji Nakamura* the Nobel Prize in Physics in 2014.[6] This award was based on their development of efficient blue light-emitting diodes (LEDs), enabling bright and energy-saving white light sources. This work was preceded by the seminal work of R. N. Hall et al.[7] on diode lasers, as well as that of Holonyak and Bevacqua[8] and Allen and Grimmeiss,[9] who developed red LEDs in the early 1960s, and that of Round[10] and Losev,[11] who reported electroluminescence from carborundum early in the 20th century. The 21st century witnessed another revolution in display technology with the development and commercialization of flat-panel displays. The technology on which these

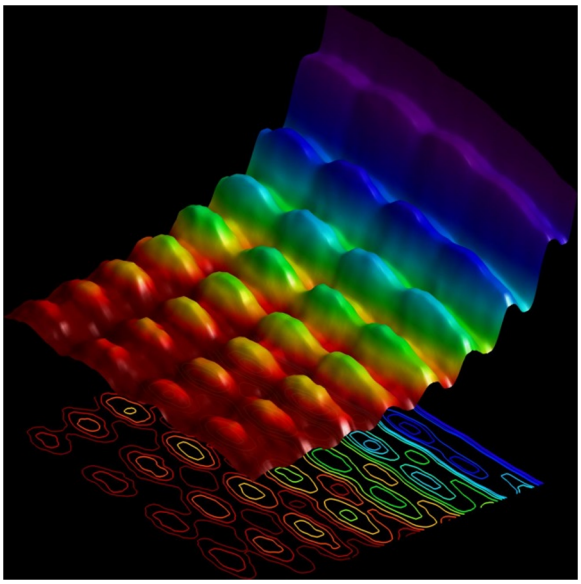

Fig. 1 Energy-space photography of light confined on a nanowire simultaneously shows both spatial interference and energy quantization.[4]

Downloaded From: http://photonicsforenergy.spiedigitallibrary.org/ on 01/26/2016 Terms of Use: http://spiedigitallibrary.org/ss/TermsOfUse.aspx

flat-panel displays is based will soon undergo another transformation with the introduction of bright, efficient, and stable organic light-emitting diodes (OLEDs).

2 Role of Photonics in Energy Conversion

The sun supplies the energy that allows all life on earth. The enormous power of the sun can be used in three main ways. The first is the conversion of sunlight to electrical power, which is discussed in Sec. 2.1. The second is the conversion of sunlight to thermal power, which is briefly described in Sec. 2.2. The third is the conversion of sunlight directly to fuels, which is the topic of Sec. 2.3. In addition, the role of photonic sensors in energy harvesting and the production of power are covered in Sec. 2.4.

2.1 *Solar Light Harvesting and Electrical Energy Conversion*

Most solar cells on rooftops now convert sunlight into electricity using the PV effect first demonstrated by Becquerel.[12] With the advent of the silicon PV cell in 1954,[13] humankind increasingly found ways of using semiconductors for many energy conversion applications. Among the first applications of solar PVs was their use in space to power control systems and other critical functions on space vehicles.[14] This subsequently grew into the application of PVs in residential solar systems for off-grid applications and has matured into grid-connected residential systems and solar power plants in the last 15 years.[15] The progress in solar PVs in terms of cell power conversion efficiencies (PCEs) can be seen in the chart from the (US) National Renewable Energy Laboratory (NREL) shown in Fig. 2. NREL makes certified measurements of PV cells, and the chart shows how different solar PV technologies have developed as a function of time (for small-area, champion solar cells). As will be explained below, the highest efficiency technologies are accompanied by very high cost and complexity, so the dominant solar cells are in the middle of the efficiency range. The newest technologies are at the bottom right of the chart, but their rapid rate of development and efficiency improvement could make them the solar PV technologies of the future. In a single-junction solar cell, the amount of light absorbed and the maximum voltage obtainable both depend on the bandgap of the semiconductor. This leads to a trade-off between the amount of light absorbed and the open-circuit voltage. The theoretical limit for the PCE of a single-junction PV cell under AM1.5 irradiation is calculated to be 33.7% using the detailed balance theory developed by Shockley and Queisser in 1961[16] and taking into account thermalization losses and low-bandgap losses in the solar cell.

2.1.1 *Inorganic solar cells*

The most important commercially available PV materials systems today are based on inorganic semiconductors. The vast majority of solar modules are based on silicon, which is the second most abundant material in the earth's crust, hence, these modules are of relatively low cost. The record silicon solar cell efficiency is 25.6%. Modules with a PCE of ~21%, fabricated by applying a thin film of amorphous silicon-based heterojunction to a silicon surface, are commercially available.[18] The majority of commercial Si modules have PCEs in the range of 14% to 18%. The modules are typically fabricated by manufacturing Si wafers with the correct doping level to form a p–n junction, along with suitable front and back contact (typically screen-printed). Both single-crystalline and multi/polycrystalline wafers are used in the industry. The cells are then laid out on a backing sheet and strung together with metal tabs. An adhesive layer is applied to bond the front glass cover, ensuring that good edge moisture barriers are also in place. Photonics plays an important role in Si-based solar cells and modules since it is an indirect bandgap semiconductor and hence has a relatively long absorption depth across the solar spectrum. Most importantly, light-trapping structures must be fashioned on the front surface of the wafers to ensure that long wavelength light is adequately trapped within the solar cell and is not lost from reflection at the back contact and subsequent impingement on the front surface (within the escape cone). Light trapping is typically achieved by etching the front surface of the wafers to form a random texture or by an anisotropic etch that forms pyramidal structures on the Si surface.[19] Another important photonic aspect of Si modules is related to the optical

Downloaded From: http://photonicsforenergy.spiedigitallibrary.org/ on 01/26/2016 Terms of Use: http://spiedigitallibrary.org/ss/TermsOfUse.aspx

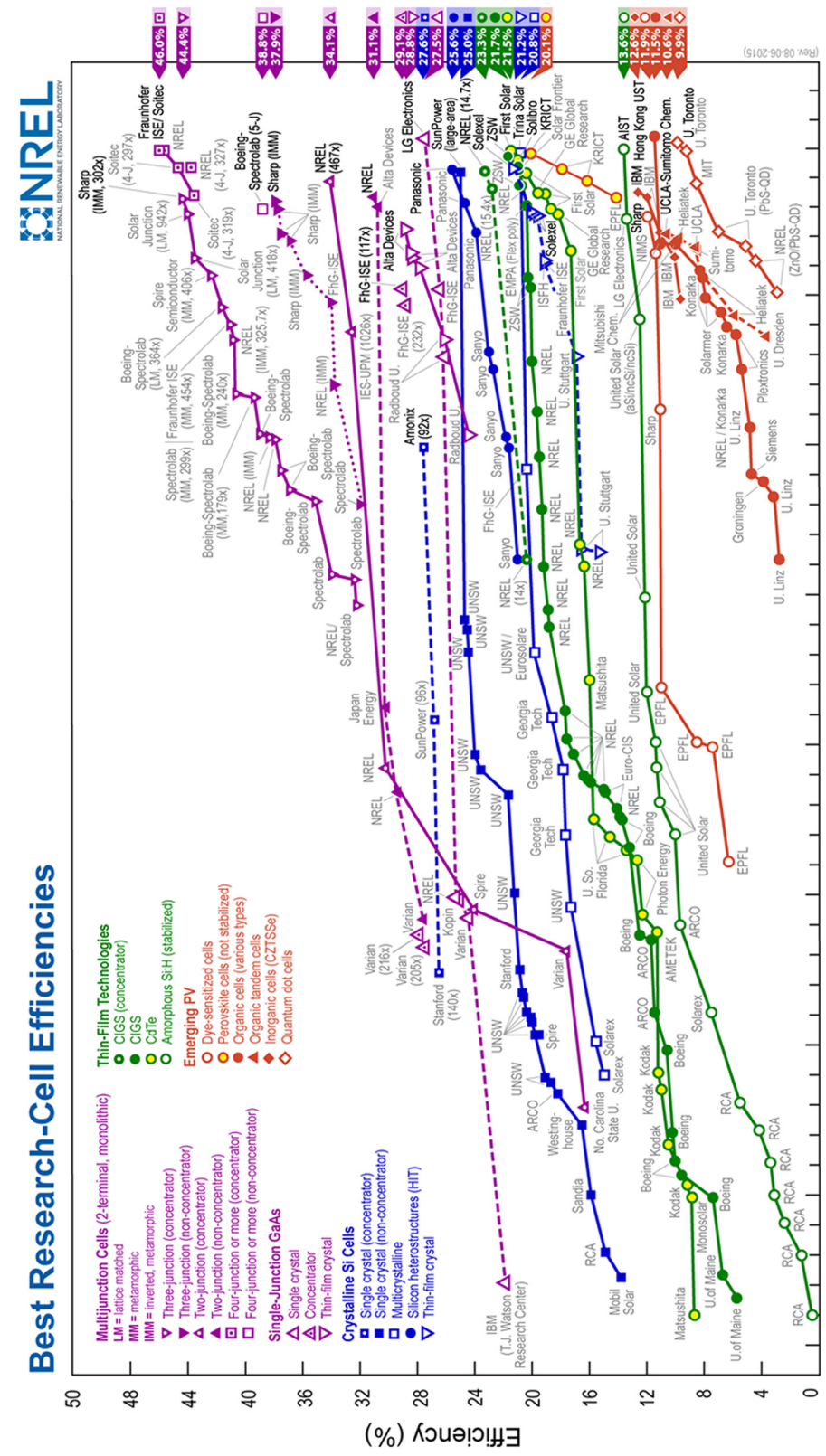

Fig. 2 Latest chart on the progress of the power conversion efficiency of solar cells reported by the National Center for Photovoltaics at National Renewable Energy Laboratory (NREL).[17]

Downloaded From: http://photonicsforenergy.spiedigitallibrary.org/ on 01/26/2016 Terms of Use: http://spiedigitallibrary.org/ss/TermsOfUse.aspx

losses that can occur at the glass/adhesive interface, as well as at the glass to air interface due to reflection. Significant advances to minimize such optical losses have been made over the last two decades.[20] Further discussion of these topics is found in Sec. 2.1.3.

Another commercially important class of materials is based on inorganic thin films, primarily related to the CdTe[21] and $Cu(In, Ga)Se_2$ (CIGS) materials systems.[22] CdTe solar cell efficiencies have been reported at 19.6% and CIGS at 20.5%. Until recently, thin-film solar cells have been lower in cost than Si solar cells due to the fact that they are direct bandgap semiconductors, and hence, a very thin layer (typically 1 to 5 μm) can be deposited using low-cost deposition processes directly onto a large-area glass substrate. This significantly lowers the manufacturing cost. One can use the glass growth substrate as the window layer, or can use it as a backing layer and add another glass window layer. In both cases, it is possible to manage the light using suitable antireflective coatings (ARC, see below).[23] Today Si and CdTe-based modules are competitive in cost (typically measured in $/Watt).

III–V semiconductor materials are also important for high-efficiency PV conversion. GaAs cells have reached 1 Sun efficiencies of 28.8%, and multijunction III–V cells have achieved an efficiency of 37.9% at 1 Sun.[18] Figure 2 gives a summary of the record efficiencies achieved by these different PV cells over the last few decades. III–V solar cells have been reserved for specialty applications, primarily for space due to their exceptionally high cost (ca. three orders of magnitude higher cost per square meter than Si). This high cost is due to several factors, including the low abundance of group III and V elements, the high expense of growing III–V crystals, the lack of a good diffusion process for forming the p–n junction (an epitaxial layer is needed), the need for another surface passivation layer to minimize surface recombination, and the need for expensive materials/processes to form good Ohmic contacts. An ARC is also always needed on the III–V surface. On the other hand, the high efficiency of III–V solar cells/modules is attributed to the direct bandgap nature of these semiconductors, which implies a short absorption depth as well as a high charge carrier mobility and high minority carrier lifetimes due to the low nonradiative losses that occur in the crystal. Surface recombination is readily minimized in III–V cell technologies by applying a suitable passivation layer. Another advantage is the fact that the bandgap of 1.5 eV gives the optimal balance of absorption of the solar spectrum and open-circuit voltage. Photon recycling in III–V solar cells has been critical in improving their performance and led to a record PCE of 28.8% for a single-junction cell.[24] Recent efforts to produce lower-cost III–V modules have allowed penetration into previously unattainable markets.[25,26]

The state-of-the-art high-performance inorganic solar cells technology is primarily pursued using multijunction stacked tandem solar cells.[27] Using materials with different bandgaps that overlap with the visible and near-IR solar spectral region leads to the absorption of photons over a wide range of energies with a small loss of photon-to-electrical energy conversion, thereby overcoming the Shockley–Queisser limit. Tandem structures require the development of appropriate absorber materials and the matching of the current density throughout all the stacked layers. Progress has been made using primarily III–V multijunction tandem cells with record efficiencies of 44.4% under concentration (302 Suns) for InGaP/GaAs/InGaAs solar multijunction cells.[27] Recent work has reported the superior lasing characteristics of GaInNAs quantum well lasers with very low threshold.[28–30] By taking advantage of this progress, the integration of III–V multijunction cells with GaInNAs-containing alloys as one of the cell materials has enabled a record PCE of 43.5%.[31] Other materials including InGaN[32] and InN[33] are currently being pursued, while others such as GaAsBi[34] are being considered for multijunction solar cells. One way of improving the cost-effectiveness of these very expensive but highly efficient solar cells is to use a concentrator, i.e., to harvest light over a large area but deliver it to small but very efficient solar cells[35] (e.g., planar Fresnel lenses[36]).

Another recent development deals with the application of various nanostructures to produce novel architectures for solar cells and, in some cases, to take advantage of new energy conversion physics. If classes of nanostructures are considered by their dimensionality, zero-dimensional quantum dots (QDs) have been applied to building new solar cell architectures that utilize quantum confinement in unique ways. For example, Green et al.[37] have proposed an all-silicon QD tandem device and are making progress toward the fabrication of such structures.[38] QDs have also been applied as novel photonic coatings that take advantage of either up- or downconversion

Downloaded From: http://photonicsforenergy.spiedigitallibrary.org/ on 01/26/2016 Terms of Use: http://spiedigitallibrary.org/ss/TermsOfUse.aspx

of portions of the solar energy spectrum in order to more effectively use bands that are lost due to thermalization or due to being sub-bandgap (and hence not absorbed).[39] One-dimensional (1-D) nanostructures, such as inorganic nanowires and carbon nanotubes, have also been explored in various novel device architectures. For example, silicon nanowires and III–V nanowire solar cells have been demonstrated[40–42] and show promise for producing low-cost, high-efficiency, flexible solar cells.[43] Two-dimensional (2-D) quantum well nanostructures have been employed to convert near-IR photons and, hence, boost the efficiency of III–V solar cells.[44] Finally, three-dimensional inorganic nanoarchitectures have been fabricated and show promising cell performance.[45]

2.1.2 *Organic and hybrid solar cells*

As depicted in Fig. 2 and discussed above, PV cells based on crystalline inorganic semiconductors have reached impressive PCEs of $> 28\%$ in single-junction and 38% in multijunction device architectures under full-sun illumination.[46] However, this class of PV cells suffers from high production and energy costs, which result in long financial and energy payback times.[47] This drawback has fostered the development of a new generation of solution-processable solar cells,[48–50] which benefit from low-cost materials (e.g., organic molecular and polymeric materials), high-throughput manufacturing methods, such as reel-to-reel coating, and low-energy expenditure.[51] This new class of PVs is referred to as emerging PV cells and can be categorized according to the materials used and mechanisms invoked: PEC or dye-sensitized solar cells (DSSCs), organic (molecular and polymer) solar cells, hybrid organic–inorganic solar cells, and QD solar cells. An overview of these emerging and promising technologies is given with the best cell PCEs achieved so far appearing at the bottom right of the NREL chart shown in Fig. 2. Since they are relatively new compared to their inorganic counterparts, it is not surprising that their efficiencies are much lower than those of the most established inorganic solar cells. However, the slope of their PCEs has been quite steep over the last few years, especially for the promising PV technology based on organic–inorganic hybrid materials (e.g., perovskites).

DSSCs, also known as PEC cells, were the first emerging PV technology to reach acceptable efficiency values. Consequently, DSSC research has initially attracted the largest number of researchers and the largest amount of industry cooperation, as well as the largest number of solar panel prototypes and related products. Since the first demonstration in 1991 by O'Regan and Graetzel,[52] and after two decades of research and development, DSSCs with an iodine/tri-iodide (I^-/I_3^-) liquid electrolyte have achieved light to electric PCEs of $> 11\%$ using ruthenium dyes,[53] $> 12\%$ based on zinc porphyrin dyes,[54] and $> 10\%$ based on metal-free organic dyes.[55] Recently, through the molecular engineering of zinc porphyrin sensitizers, Grätzel and coworkers have reported solar cells with 13% PCE. The new sensitizers feature the prototypical structure of a donor–π-bridge–acceptor, maximize electrolyte compatibility, and improve light-harvesting properties.[56] Using SM315 dye with the cobalt (II/III) redox shuttle resulted in DSSCs that exhibit a high open-circuit voltage (V_{OC}) of 0.91 V, short-circuit current density (J_{SC}) of 18.1 mA cm^{-2}, and a fill factor (FF) of 0.78. However, there are several problems that limit the mass production and long-term stability of such devices, such as leakage and evaporation of the liquid electrolyte, and corrosion of the metal-based current collectors (silver, copper, etc.) by iodine. As a result, substantial effort has been made to find alternative electrolytes and/or introduce new concepts to develop electrolyte-free DSSCs. In solid-state DSSCs (ss-DSSCs), the liquid electrolyte is entirely replaced by a solid organic hole transport material (HTM). For the solid-state version (ss-DSSC), PCEs $> 20\%$ have been predicted,[57] using low-cost materials,[58] low temperature processing (< 150°C), and reel-to-reel fabrication methods.[59,60]

Organic (molecular and polymeric) solar cells represent another and different category in the class of emerging PVs. These solid-state devices have attracted a lot of attention in the last 20 years as one of the most promising technologies for low-cost solar energy conversion. A key difference from their inorganic semiconductor counterparts results from their low dielectric constant and gives rise to strongly bound upon solar light absorption at room temperature. A chemical potential is required between the hole (p-type) transporter/electron donor and the electron (n-type) transporter/acceptor in order to separate the photogenerated carrier charges and

Downloaded From: http://photonicsforenergy.spiedigitallibrary.org/ on 01/26/2016 Terms of Use: http://spiedigitallibrary.org/ss/TermsOfUse.aspx

often involves the use of a strong electron acceptor. One subclass of these devices is based on a light-harvesting material that consists of a mixture of a conjugated polymer as the p-type material or hole transporter/electron donor and a fullerene derivative as the n-type material or electron transporter/acceptor. The operating mechanism in these organic solar cells, discovered in the mid-1990s by Sariciftci et al.,[61] is based on photoinduced electron transfer from a conducting polymer such as a poly(*p*-phenylene vinylene) (PPV) derivative to a fullerene derivative. This finding opened up a very rich and intensive research field involving the synthesis of new conjugated polymers and copolymers with low-bandgap and high charge carrier mobilities, novel fullerene derivatives with better solubility, morphology control of the active light-harvesting layer, and different solar cell configurations. In particular, the so-called bulk heterojunction (BHJ) in which the donor and acceptor are mixed together is most widely used because it enables efficient charge generation even in materials with very limited exciton diffusion length. Further refinements included novel contact materials aiming to give better interfaces for electron and hole collection, and the investigation of ground and excited states to understand the complex mechanisms involving exciton formation and diffusion, charge-transfer state formation and separation followed by charge transport and collection.

Organic solar cells with BHJ architectures using conducting polymers and fullerene molecules are by far the most studied,[62,63] achieving PCEs close to 10% using one polymer as an absorber (i.e., single-junction devices), in both regular and inverted device structures.[64–67] The chemical nature of the electron donor polymers has evolved from simple structures, such as PPV and poly(3-hexylthiophene) (P3HT), to more complex copolymers specially designed to have both electron donor and acceptor groups in their structures in order to reduce their bandgap. One example is the newly synthesized narrow-bandgap semiconducting polymer poly [[2,6′-4,8-di(5-ethylhexylthienyl)benzo[1,2-b;3,3-b] dithiophene] [3-fluoro-2[(2-ethylhexyl)carbonyl]thieno [3,4-b]thiophenediyl]], which when used in the light-harvesting layer led to a very efficient cell that delivered a certified PCE of 9.94%.[67] Recently, Yang and coworkers have fabricated a multijunction solar cell having a PCE exceeding 11%, suggesting great potential for tandem architectures in organic photovoltaic (OPV) research[68] (see Fig. 3).

Small molecules offer some advantages over conducting polymers, such as synthetic flexibility, ease of purification, less batch-to-batch variation in properties, higher hole and electron mobilities in some cases, and intrinsic monodispersity. Efficient molecular BHJ solar cells have recently been reported in which merocyanine dyes, squaraine dyes, fused acenes, triphenylamine, benzofuran benzothiadiazole, diketopyrrolopyrrole, benzodithiophene, and other chromophores, such as oligothiophenes and push-pull organic dyes, have been employed as the

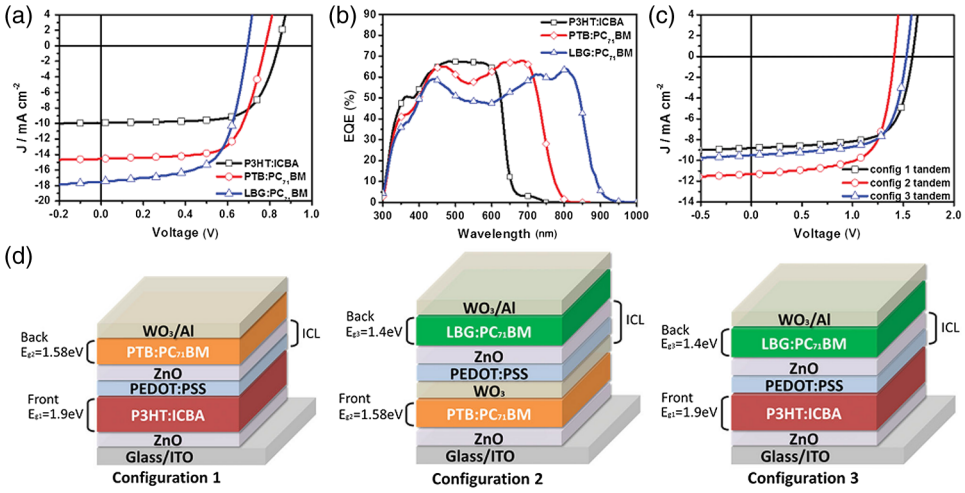

Fig. 3 (a) $J-V$ characteristics and (b) action spectra, external quantum efficiency as a function of wavelength, for single-junction photovoltaic (PV) cells based on poly(3-hexylthiophene):ICBA, PTB:[6,6]-phenyl-C71 butyric acid methyl ester ($PC_{71}BM$), and LBG:$PC_{71}BM$ as the active light-harvesting layers. (c) $J-V$ characteristics and (d) device configurations (front subcell/back subcell) of inverted double-junction tandem OPVs. (Reproduced with permission from Ref. 68 © 2014 WILEY-VCH Verlag GmbH & Co. KGaA, Weinheim.)

Downloaded From: http://photonicsforenergy.spiedigitallibrary.org/ on 01/26/2016 Terms of Use: http://spiedigitallibrary.org/ss/TermsOfUse.aspx

light-harvesting donor components.[69–71] State-of-the-art OPV devices achieved PCEs up to 10%.[72–75] Recently, molecular OPVs based on oligothiophenes with five thiophene units in the backbone and 2-(1,1-dicyanomethylene)rhodanine as end capping units exhibited a PCE of 10%.[76]

State-of-the-art solution-processed devices generally rely on the BHJ of polymer electron donors and fullerene electron acceptors.[77] Fullerene derivatives, such as [6,6]-phenyl-C_{61} butyric acid methyl ester ($PC_{61}BM$) and [6,6]-phenyl-C_{71} butyric acid methyl ester ($PC_{71}BM$), have played a leading role as electron acceptor materials; however, they suffer from poor absorption in the visible and near-IR regions. Recently, nonfullerene electron-accepting chromophores, such as perylene diimide, naphthalene diimide, vinazene, fluoranthene-fused imide, benzothiadiazole, rhodanine, and diketopyrrolopyrrole, have been incorporated with success in BHJ molecular and polymeric solar cells.[78–84] So far, state-of-the-art BHJ devices based on nonfullerene acceptors have shown PCE up to 6%.[84]

Hybrid organic–inorganic solar cells have structures similar to the cells described above where the electron-accepting fullerenes are substituted with inorganic semiconductors (e.g., TiO_2, ZnO, $CuInS_2$, PbS, CdSe, and CdTe) nanoparticles.[85–88] Chalcogenide nanoparticles with quantum confinement properties have also been considered and used as sensitizers in DSSCs.[89,90] These solar cells offer a series of advantages over the more traditional BHJ OPVs based on the polymer/fullerene systems. Some of the expected advantages are (1) a contribution to light absorption by an inorganic acceptor can lead to the generation of more photocarriers, due to their larger linear absorption coefficients compared to those of fullerene derivatives; (2) the absorption of nanoparticles can be tuned to cover a broad solar spectral range, as a result of modification of their size and shape, complementary to that of the organic electron donor/hole transporter; (3) the physical dimensions of some inorganic semiconductors can be tailored to produce 1-D nanostructures, to allow efficient exciton dissociation, i.e., charge separation and electron transporting pathways simultaneously; (4) ultrafast and efficient photoinduced charge carrier transfer between the electron acceptor (inorganic nanoparticles) and the electron donor (the organic semiconductor); (5) the acceptors have relatively high electron mobility; and (6) good photo- and chemical stability.[91] However, to date, PCEs achieved for hybrid organic–inorganic solar cells are significantly lower than those of OPV devices, which is primarily due to the challenges in controlling the interface between the nanoparticles and the polymer, and achieving a well-defined matrix with a continuous percolation network. Furthermore, the presence of surface traps on the nanoparticles can be problematic for achieving good charge generation and carrier transport. An efficiency of 3.5% has been achieved in a BHJ architecture when combining CdSe nanorods and PbS QDs with different polymers.[92,93] More recently, silicon and an organic polymer (e.g., P3HT) and carbon nanotubes have been combined to give hybrid solar cells with efficiencies reaching 11%.[94,95]

A recent breakthrough occurred in the last couple of years with the demonstration of highly efficient solar cells based on organic/inorganic lead halide perovskite absorbers. These light-harvesting organic–inorganic materials have transformed the field of organic/inorganic hybrid PV devices.[96,97] Solution processed PVs incorporating perovskite absorbers, such as $CH_3NH_3PbI_3$ and $CH_3NH_3PbI_{3-x}Cl_x$, have achieved efficiencies of 20.1% (certified, but not stabilized) in solid-state device configurations, surpassing liquid DSSCs, evaporated and tandem organic solar cells, as well as various thin-film inorganic PVs, thus establishing perovskite-based solar cells as a robust candidate for expanding the worldwide PV market. In 2009, hybrid perovskites were first used in the work of Kojima et al.[98] as the sensitizer (absorber) in a DSSC with liquid electrolyte, generating only a 3.8% efficiency. The breakthrough, however, came in 2012 when the group of Snaith at the University of Oxford and the group of Grätzel at EPFL combined the perovskite with the well-known DSSC solid-state HTM, 2,2′,7,7′-tetrakis(*N,N*-di-*p*-methoxyphenyl-amine)-9,9′-spirobifluorene (spiro-OMeTAD).[99,100] The Oxford group demonstrated that a mesoporous TiO_2 scaffold is not necessary and that the hybrid perovskites are able to transport both electrons and holes. In subsequent reports, efficiency values of 15% were attained in different systems with various morphologies, either in nanoheterojunction or planar thin-film configurations with different chemical compositions and preparation routes.[101–106] To date, efficiency values exceeding 16% have been reported with two quite different configurations, using $CH_3NH_3PbI_3$ perovskite in a classical solid-state DSSC and in a thin-film planar configuration

Downloaded From: http://photonicsforenergy.spiedigitallibrary.org/ on 01/26/2016 Terms of Use: http://spiedigitallibrary.org/ss/TermsOfUse.aspx

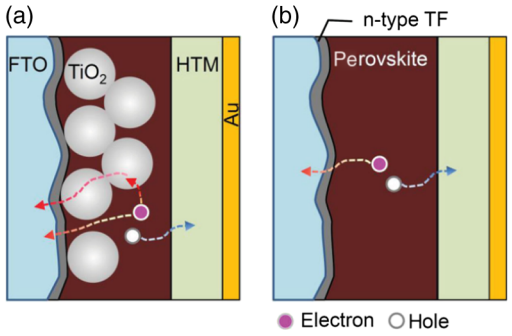

Fig. 4 (a) Mesoscopic perovskite solar cell with mesoporous TiO_2 layer and (b) planar structure without a mesoporous TiO_2 layer. Thin film on fluorine-doped tin oxide (FTO) is an n-type semiconductor. HTM stands for hole transporting material. In the mesoscopic structure, electrons can be collected directly and/or via TiO_2 layer. (Reproduced with permission from Ref. 115 © 2014 WILEY-VCH Verlag GmbH & Co. KGaA, Weinheim.)

with $CH_3NH_3PbI_{3-x}Cl_x$, as shown in Fig. 4.[107,108] The use of a mixed solvent of γ-butyrolactone and dimethylsulfoxide followed by toluene drop-casting leads to solar cells with a certified PCE of 16.2% and no reported hysteresis.[109] The lack of hysteresis, which had been an obstacle for the stable operation of perovskite devices, was observed recently using thin films of organometallic perovskites with millimeter-scale crystalline grains with efficiencies close to 18%.[110] Stabilization of the perovskite phase based on formamidinium lead iodide ($FAPbI_3$) with methylammonium lead bromide ($MAPbBr_3$) as the light-harvesting unit in a bilayer PV architecture improved the PCE of the solar cell to $> 18\%$.[111] Interestingly, electron transport layer-free and hole transport layer-free perovskite solar cells have also been reported, simplifying the device structure, thus opening up an interesting route to low-cost production of solar cells.[112–114]

The excellent PCEs achieved for solar cells based on perovskites are attributed to their long extended electron–hole diffusion length ($> 1\ \mu$m),[116,117] broad solar light absorption (visible to near-IR), good solubility in organic media, and high carrier mobility. However, identifying the basic working mechanisms, which are still being debated, improving film quality, and improving device stability are important challenges that need to be addressed before serious consideration for their future development and commercialization.

Colloidal QD thin-film solar cells (CQD cells), depicted in Fig. 5, are also part of the newly emerging PV technology. These devices have the potential to reduce manufacturing costs due to their solution processability, light weight, and being amenable to large area deposition. CQDs can be utilized in Schottky,[118,119] p–n heterojunction,[120,121] hybrid BHJ,[91] and as the sensitizers in PEC solar cells.[122] CQDs are nanometer-sized particles that are below the Bohr exciton radius of the specified material. CQDs are synthesized by rapid injection of the reactant into the reaction medium with stabilizing agents under an inert gas atmosphere. The role of the stabilizing agent, such as oleic acid and oleylamine, is to control growth rate, particle size, and dispersion of

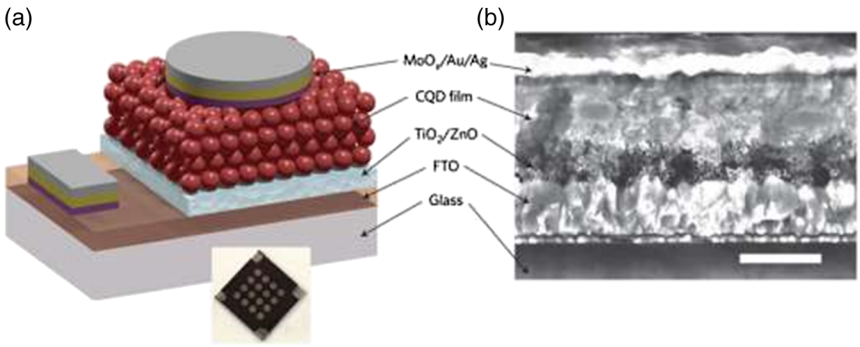

Fig. 5 (a) Schematic diagram and (b) cross-sectional scanning electron micrograph (SEM) of a colloidal quantum dot (CQD)-based organic photovoltaic device with a PbS CQD film and TiO_2/ZnO junction. (Reprinted with permission from Ref. 118 © 2012 Macmillan Publishers, Ltd: Nature Nanotechnology.)

Downloaded From: http://photonicsforenergy.spiedigitallibrary.org/ on 01/26/2016 Terms of Use: http://spiedigitallibrary.org/ss/TermsOfUse.aspx

the QDs. However, it may hinder the route for high-efficiency CQD-based PVs. The reduction of the interparticle spacing and passivation of surface traps in CQDs remain as primary challenges.

Among several candidates, PbS CQDs are of interest due to their ease of bandgap tunability in the visible region, and their simple, high-yield synthesis. Sargent[122] and McDaniel et al.[123] showed that performing a hybrid ligand exchange (long organic ligands are replaced simultaneously by short ligands and by halide ions, e.g., $CdCl_2$) results in efficient CQD solar cells in a p:n configuration with metal oxides (TiO_2, ZnO). The PCE was improved to 8.5% by reducing the TiO_2 thickness layer to 10 nm in order to increase the depletion width.[124] As CQD and perovskite solar cells develop further, their environmental impact will need to be considered, leading to a search for lead and cadmium free materials.

2.1.3 *Light management in solar cells*

An essential function of photonics is to optimize light coupling into PV device and to improve light trapping within the absorbing light-harvesting layer. Since solar power converters primarily rely on inorganic semiconductors, there is a significant discontinuity in the refractive index between air or the encapsulant material, and the silicon or other inorganic semiconductors, such as III–V (e.g., GaAs, InP, etc.) and II–VI (e.g., CdTe) compounds—the discontinuity in the refractive index can be as high as 4.[125] This refractive index discontinuity leads to significant Fresnel reflection losses at the interface across the solar spectrum that can reduce the performance (i.e., PCE and energy yield) of the solar energy conversion system. It should also be noted that, in reality, a PV module consists not only of the semiconductor device, but also of various protecting layers, such as glass and protective/adhesive transparent polymers, and hence, the full module must be considered as an optical system when designing proper light-management approaches.[20,126]

The most widely used photonic method for minimizing reflection losses from the semiconductor surface is the single-layer or double-layer ARC.[127] These coatings are typically designed to minimize the reflection via interference of optical plane waves and consist of thin, transparent films of silicon nitride, silicon oxide, titanium oxide, and other similar compounds. Of course, it is possible to design more advanced multilayered ARCs to further minimize reflection losses; however, for solar PV applications, this is typically too costly to implement. It is noted that such ARCs are deployed directly on the active solar cell and are then embedded within the polymer adhesive used to bind the protective glass cover for the solar module. Note that the glass itself, being a dielectric in the UV to near-IR portion of the solar spectrum, has a much lower refractive index than silicon, and hence, the outer module reflection loss is lower, i.e., ca. 4% reflection loss. Nevertheless, in recent years, glass manufacturers have also started to implement ARCs on the outer surface of the module, which, of course, provides additional requirements on the durability of the coating from mechanical handling during manufacturing and installation to environmental effects in the field, such as erosion.[128]

As the solar industry expanded rapidly in the last decade, it became apparent that thin-film ARCs have limitations with regard to their performance. This has to do with the fact that the reflection is often minimized for only a select region of the solar spectrum and also has a strong dependence on the angle of incidence. The surface reflectance increases rapidly as sunlight goes from normal incidence to high angles that arise during the morning and evening hours, which can lead to significant (up to ca. 30%) energy production losses.[129] One solution is to have an active system that tracks the sun (see Sec. 2.4.1), but such systems are expensive and complicated, so passive systems that reduce these losses are of considerable interest. In recent years, the application of nanostructured surfaces (e.g., micro- or nanopillars or nanowires) that can be used to minimize reflection across the full solar spectrum and also up to high angles has been explored to address this problem.[130,131] These structures typically produce a graded effective refractive index that leads to an ultralow, broadband reflection that is also omnidirectional; hence, these structures have been categorized as being omnidirectional antireflective (ODAR) layers.[132] A related concept has been to develop ODAR layers that can also act as downconverting layers, hence better optimizing the spectrum that the semiconductor absorbs to avoid thermalization losses when high-energy photons are absorbed.[133]

Downloaded From: http://photonicsforenergy.spiedigitallibrary.org/ on 01/26/2016 Terms of Use: http://spiedigitallibrary.org/ss/TermsOfUse.aspx

Indeed, downconversion is part of a broader light-management strategy being investigated by researchers worldwide to more effectively utilize the solar spectrum. High-energy (short wavelength) photons lead to thermalization losses when charge carriers are excited above the conduction band edge. Alternatively, low-energy photons (long wavelengths) are not absorbed by the semiconductor and, hence, also lead to losses with respect to what the PCE of the solar cell could be if these photons were properly utilized. Calculations have shown that the limiting efficiency of a single-junction solar cell could go from 30.9% to 39.6% using a downconverting (or so-called quantum cutting) layer on the surface of the solar cell, whereas using an upconverting layer on the backside of the solar cell can increase the limiting efficiency (under 1 Sun illumination) to 47.6%.[134,135] Research has focused on developing new optically active materials that can achieve up- or downconversion (e.g., QDs).[38,136]

In addition to minimizing surface and interface reflections, light-trapping methods have become important as the light-harvesting active layers have become thinner over the past few decades (thicknesses are approaching a few tens of microns for silicon-based solar cells; are on the order of a micron or less for thin-film inorganic solar cells; and are in the region of 10 to 100 nm for organic solar cells). When the semiconductor active layers become thinner, material costs are reduced and, in some cases, the electrical properties are improved (e.g., due to reduced bulk electron–hole recombination). However, the optical density of the active layer is reduced and in-coupled solar radiation may not be fully absorbed during the first (or second) pass of light through the material. Therefore, methods to trap or increase the path length of light within the semiconductor layer have been developed to increase the effective optical density of the material.[137,138] The use of highly reflective back electrodes, textured back reflectors or electrodes, and textured semiconductor surfaces has been found to improve light trapping and, hence, the PCE in a host of PV devices. However, there is a limit (known as the ergodic or light-trapping limit) to the number of passes that light can take within a thin-film active layer using textured surfaces or back reflectors, which is proportional to $4n^2$.[139,140] Approaches have been demonstrated that break this limit over relatively narrow wavelength ranges using photonic crystals (PCs), dielectric micro and nanostructures, and other photonic and plasmonic nanostructures.[141] For light trapping over the broad solar spectrum in thin-film PVs, texturing of back reflectors and semiconductor surfaces is still the most practical approach. Besides light trapping, for semiconductor materials with fast radiative recombination rates [high internal quantum efficiencies (QEs)], such as GaAs, photon recycling by means of highly reflective back electrodes and controlling interference effects within the active layer have enabled record single-junction solar cell PCEs.[26,142,143]

With the development of thin-film optoelectronic devices that have active layer thicknesses below the diffraction limit (i.e., $< \sim 300$ nm); such as small molecule and polymeric OPVs in which the active light harvesting layer thickness ranges from $\sim$10 to 40 nm and up to $\sim$250 nm, respectively, light-management techniques using nanophotonic structures, particularly metallic plasmonic structures, have emerged.[144–156] Metal nanoparticles and structured metallic thin films can localize incident light to subwavelength dimensions due to the excitation of surface plasmons—collective electron oscillations of the free electrons at the surface of metals. However, for such effects to be strong, the metals must exhibit weak intra and interband electronic absorption losses. Therefore, noble metals are typically used for subwavelength thin-film light management using plasmonics. However, even noble metals behave as nonideal metals at optical frequencies; therefore, parasitic absorption loss is always present to some degree. Despite these losses, well-designed plasmonic nanostructures can greatly improve light harvesting for a range of energy applications that employ very thin layers or small absorber material volumes.

For example, arrays of discrete plasmonic nanoparticles and nanoantennas have been shown to effectively harvest and localize incident light within semiconductor thin films and, therefore, improve light absorption and electron–hole pair generation rate at the nanoscale. Far-field scattering by such nanostructures placed on top of or within thin-film PV devices have been shown to improve short-circuit current densities by $\sim$20% to 70% (compared to analogous devices without the plasmonic nanostructures) through the increased effective path length of incident solar radiation with the semiconductor absorber layer.[145–151] Optimization of the albedo (ratio of scattering crosssection to extinction cross-section), location, degree of shadowing, and shape of the nanostructures is typically required to achieve significant improvements in short-circuit current

Downloaded From: http://photonicsforenergy.spiedigitallibrary.org/ on 01/26/2016 Terms of Use: http://spiedigitallibrary.org/ss/TermsOfUse.aspx

density. In addition to far-field scattering, near-field localization or trapping of incident light into guided surface plasmon polariton modes at the metal/semiconductor interface using nanostructured metal electrodes, such as nanotextured or nanopatterned metal thin films and metasurfaces, is also of interest for increasing the effective absorption depth of semiconductor thin films.

Additionally, (semi)transparent metal nanowire arrays and nanohole arrays can both facilitate light trapping and in-coupling to guided surface plasmon polariton modes and also act as transparent electrodes.[148,157–161] Near-field localization using the aforementioned structures and using plasmonic nanoantenna structures has also been found to increase the generation rate of electron–hole pairs, which can lead to increased PCE in thin-film PV devices. More recently, photosensitization of wide-bandgap semiconductors and generation and collection of hot electrons on plasmonic nanostructures were shown to be an alternative means to harvest solar energy for applications in PVs, photocatalysis, and solar-to-fuel energy conversion.[152,162–164] Plasmonic absorber materials have also been considered for light harvesting without the need for semiconductor materials.[165,166]

2.2 *Solar Light Harvesting and Thermal Energy Conversion*

An important alternative to converting sunlight to electricity is to harvest the thermal energy directly where photonics also plays an important role. One simple application involves the use of concentrated solar power, where sunlight is focused onto long pipes coated with an optically absorbing material and filled with a high-thermal capacity fluid, which is used to drive a turbine.[167,168] From a photonics perspective, the emphasis has been on the development of advanced coatings with high absorption coefficients in the UV to the IR solar spectral region, which included the development of carbon nanotube and metallic nanowire arrays,[169,170] as well as PCs,[171] with the goal to create nearly perfect black absorbers. The solar thermal concept has also been applied to a vertical configuration in which a circular array of mirrors is used to concentrate reflected sunlight onto a solar tower that uses heat to generate electricity.[172] More commonly, sunlight is widely used (without concentration) for domestic water heating.

The progress made in solar PVs has enabled relatively efficient conversion of solar photons into electrons for electricity generation. In addition, it has opened up an interesting alternative way of converting thermal energy into electrical energy, namely thermophotovoltaics (TPVs). The basic principle of a TPV system, illustrated in Fig. 6, lies in heat supplied to an emitter leading to the emission of thermal radiation (photons). Thermally generated photons of sufficient energy are then absorbed in the TPV cell leading to the generation of electrons and holes, just as in a conventional PV device.[173] A filter/reflector is used to transmit only photons of energy greater than the bandgap of the TPV cell and reflect lower-energy photons back onto the emitter so that their heat is recycled. The design of such a system involves optimizing three key components, where the first one is the heat source, which serves as the thermal blackbody radiation emitter. By identifying the temperature of the emitter, the peak wavelength of the blackbody radiation can be obtained, which in turn defines the choice of the semiconductor for the TPV cell. The filter/reflector needs to be designed to match the spectral properties of the emitter

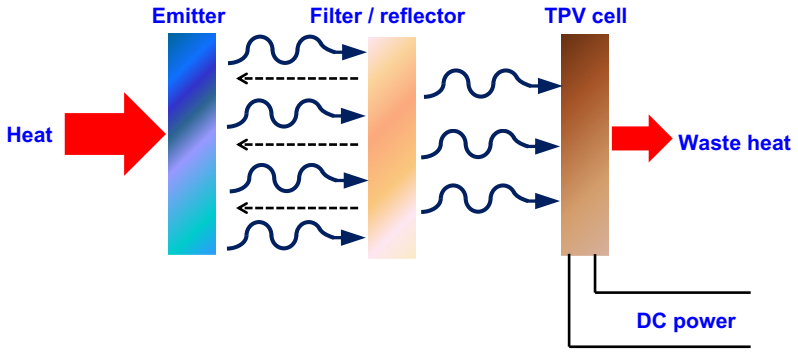

Fig. 6 Schematic of thermophotovoltaic systems including emitters, filter, and absorber PV materials.

Downloaded From: http://photonicsforenergy.spiedigitallibrary.org/ on 01/26/2016 Terms of Use: http://spiedigitallibrary.org/ss/TermsOfUse.aspx

and the TPV cell. This is achieved using PCs or multilayer structures where one can design a long-pass filter with precise sets of cut-off wavelengths.

The key applications of TPVs include the space station, cars, and heavy industries. The thermal radiation of interest has a temperature operation around 1000 to 1500 K, which corresponds to cut-off wavelengths of ~2 to 3 μm. For ensuring the stability of the emitters, the TPV emitters are commonly based on rare earth oxides, silicon carbide, and tungsten. In order to harness the thermal energy, the materials of interest for the TPV devices are based on inorganic semiconductors, such as Si and III–V alloys. More specifically, the use of GaSb and InGaAsSb is of great interest since their bandgaps can be tuned over the wavelength range of interest.[174] Such state-of-the-art materials (e.g., GaSb) are used with antireflection-coated tungsten foil on alumina design for the emitter in TPVs with an electrical efficiency of 10.6%.[175] Progress in GaSb and InGaAsSb lasers[176] has also fueled tremendous improvement in the quality of materials relevant to the TPV applications. In addition, recent work on both dilute-nitride and dilute-SbN material systems has shown promise to push into the wavelength regime for TPV,[177–180] where the use of dilute-bismuthide materials as absorbers in the 2 to 3 μm spectral region has shown promise.[181] For the emitter, a 2-D tantalum PC has been used, and an electrical efficiency up to 16% is predicted.[182] Another approach employs a graded-index tungsten emitter structure to enhance the spectral efficiency in the solar TPV system.[183] Future advances will result from the development of materials and the structure design of the emitters, filters, and PV cells to optimize the radiant efficiency and spectral and infra-red photon to electron conversion efficiencies of the PV cells in the TPV systems.

Thermoelectric materials offer an alternative approach to harness thermal energy by conversion of heat into electricity using the Seebeck effect.[184] Recent work has focused on nanostructures and alloys to improve the thermal energy conversion in thermoelectric systems.[185–189]

2.3 *Solar Light Harvesting, Chemical Energy Conversion and Fuel Generation*

Research on solar fuels accelerated dramatically when Fujishima and Honda[190] demonstrated that water photochemically splits into hydrogen and oxygen at titanium dioxide (TiO_2) photoelectrodes illuminated with sunlight. The findings presented both enormous opportunities and challenges: TiO_2 is both cheap and chemically durable, making it appealing as a photocatalyst and photoelectrode material, but the efficiency of sunlight-driven water splitting at unmodified TiO_2 is poor. The two most common polymorphs of TiO_2, rutile and anatase, both require excitation with ultraviolet (UV) light to create excited state electron–hole pairs that drive photochemical reactions (Fig. 7). UV light comprises < 5% of the terrestrial solar spectrum. Immeasurable effort has been exerted to improve the utilization of both UV and visible light

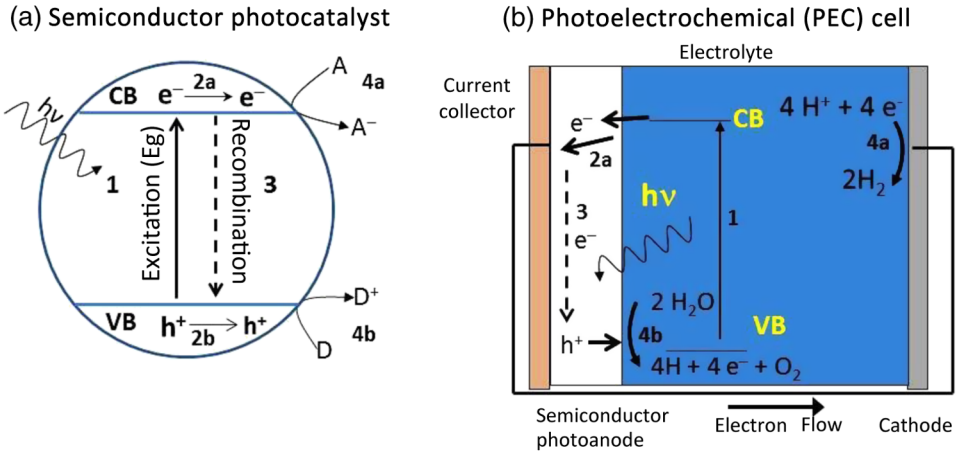

Fig. 7 Schematic representation of photocatalysis at (a) dispersed semiconductor materials; and (b) in a photoelectrochemical water-splitting cell.

Downloaded From: http://photonicsforenergy.spiedigitallibrary.org/ on 01/26/2016 Terms of Use: http://spiedigitallibrary.org/ss/TermsOfUse.aspx

by sensitizing TiO_2 with dyes, atomic dopants, plasmonic metal nanoparticles, and semiconductor nanocrystals, as well as by rendering it as high surface area nanostructured materials and nanoparticles.[191–193] Visible light active photocatalysts derived from semiconductors with narrower bandgaps have also been extensively investigated.[194–196]

Photocatalysis at dispersed semiconductor powders [Fig. 7(a)] or semiconductor photoelectrodes [Fig. 7(b)] requires that the semiconductor absorbs a sufficiently energetic photon to promote an electron from the valence band (VB) to the conduction band (CB) of the semiconductor (step 1). After creation of the electron–hole pair, the CB electron and VB hole must each diffuse to the semiconductor surface (step 2) before the electron–hole pairs relax via recombination pathways, removing them from the photochemical process (step 3).

Upon reaching the semiconductor surface, the electron and hole react (step 4) to reduce the electron acceptor molecules (A) and oxidize the electron donor molecules (D). In photocatalytic water splitting, H_2O acts as the electron donor and is split into oxygen and protons (H^+), while transferring the electrons to the semiconductor [Eq. (1)]. Protons are reduced by the CB electrons of the semiconductor to yield molecular hydrogen [Eq. (2)]:

$$2H_2O \rightarrow 4H^+ + 4e^- + O_2, \tag{1}$$

$$4H^+ + 4e^- \rightarrow 2H_2. \tag{2}$$

Several recent reviews extensively describe the various approaches to achieving photocatalytic water splitting.[197–205] Because both the photocatalytic oxidation step [Eq. (1)] and reduction step [Eq. (2)] are catalytically challenging in pure water, the activity of new oxidation or reduction cocatalysts (typically either catalytic noble metal nanoparticles or molecules attached to the semiconductor surface) for the individual half reactions are typically studied in isolation. To evaluate hydrogen generation kinetics [Eq. (2)], an easily oxidized sacrificial electron donor, such as methanol, is often added to the reaction to remove the kinetic bottleneck comprising water oxidation [Eq. (1)]; when evaluating oxidative water splitting, an electron acceptor is added to the reaction to remove the effects of slow hydrogen generation kinetics, especially in neutral or basic conditions, when proton concentration is low.

Typical values for apparent QE for H_2-generation via visible light driven photocatalytic splitting of H_2O are $< 1\%$,[197] with the notable exception of the work by Domen and coworkers, who report QE of 2.5% with gallium nitride/zinc oxide modified with rhodium chromate,[206] and zinc-germanium oxynitride semiconductor materials modified with ruthenium oxide[207] cocatalysts. The reason that photocatalytic efficiency for water splitting in pure H_2O using visible light remains generally poor is that very few photocatalysts perform all of the steps depicted in Fig. 7 well enough to successfully execute the entire process efficiently.

2.3.1 *Tandem photoelectrochemical/photovoltaic devices for water splitting*

The often orthogonal requirements for good light-harvesting efficiency, charge separation, and catalytic reaction efficiency suggest that unburdening the catalytic material from at least one of these steps could enable solar fuel processes to run more efficiently. Khaselev and Turner[208] developed a tandem PEC/PV system that separated the light harvesting and photovoltage generation from the catalytic water oxidation processes (while still driving reductive hydrogen generation at the photoelectrode). The energy efficiency for H_2-generation under simulated sunlight—defined as the ratio of the energy value of H_2 produced to the total energy of absorbed light—was 12.4%. The practical drawback of their device (Fig. 8) is that the PV element was an expensive, epitaxially grown n–p–n GaAs/GaAs/GaInP device. In the same year, Rocheleau et al.[209] described a tandem PEC/PV system using cheaper amorphous silicon as the active material in the triple-junction PV and reported solar-to-H_2 efficiencies of 7.5% to 7.8%. Very recently, Cox et al.[210] demonstrated 10% solar-to-H_2 efficiency with tandem PEC/PV devices using inexpensive commercial solar cells based on crystalline Si on the PV side and low-cost hydrogen and oxygen generation catalysts in the PEC. This tandem approach coupled with state-of-the-art nonprecious catalyst materials has been dubbed the artificial leaf.[211]

Downloaded From: http://photonicsforenergy.spiedigitallibrary.org/ on 01/26/2016 Terms of Use: http://spiedigitallibrary.org/ss/TermsOfUse.aspx

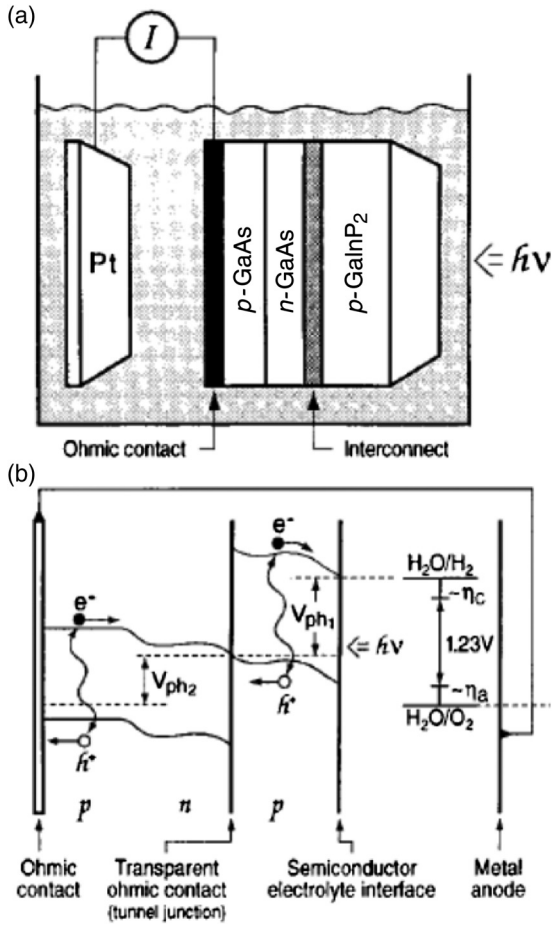

Fig. 8 (a) Schematic of the monolithic PEC/PV device. (b) Idealized energy level diagram for the monolithic PEC/PV photoelectrolysis device. (Reproduced with permission from Ref. 208. Copyright AAAS.)

Given the much higher efficiencies for solar H_2-generation from water achieved at tandem PEC/PV devices (> 10% solar-to-H_2 energy efficiency under simulated sunlight) compared to those measured for dispersed photocatalysts illuminated with visible light (typically < 1% QE, which translates into still lower solar-to-H_2 energy efficiency), the question arises as to whether solar fuels photochemistry at dispersed photocatalysts has already lost the technological race. As the price of PV devices decreases, the tandem approach becomes increasingly attractive. However, dispersed semiconductor nanomaterials can separate electrons and holes extremely rapidly, and if durable, cost-effective means of improving the efficiency of the cheapest semiconductor photocatalyst materials, such as TiO_2 and iron oxides, are discovered, dispersed photocatalytic materials could conceivably emerge as the more cost-effective technologies.

2.3.2 *Liquid fuel production via photocatalytic CO_2 reduction*

While the recent advances in H_2-generation photocatalysis are tremendously important, the infrastructure for storing and using H_2 as a use-flexible fuel supply still does not exist. In the near term, liquid fuels will continue to comprise a substantial portion of the world fuel supply, particularly in the transportation sector. The photocatalytic reduction of CO_2 to fuels and fuel precursors is still more difficult than photocatalytic water splitting. The photochemistry follows the same general pathway outlined in Fig. 7(a), with the final reduction step [Fig. 7(a), step 4a] being the slow, inefficient reduction of CO_2 to the most desired products, either CH_4 or CH_3OH. Side products—wanted or unwanted—typically include a mixture of H_2, CO, and

Downloaded From: http://photonicsforenergy.spiedigitallibrary.org/ on 01/26/2016 Terms of Use: http://spiedigitallibrary.org/ss/TermsOfUse.aspx

HCOOH. If photocatalytic CO_2 reduction is also truly to be carbon-neutral, the initial oxidation chemistry (step 4b) should use H_2O as the electron donor. In short, photocatalytic CO_2 reduction involves all of the difficult steps of photocatalytic water splitting, with a particularly onerous reduction step added at the end of the catalytic process.

Like catalysts for photochemical water splitting, photocatalytic CO_2 reduction and semiconductor-based photocatalysts have been extensively reviewed in the past few years.[212–217] Considerable effort has been focused on both TiO_2-based photocatalysts[212,216] and on alternative semiconductors to TiO_2.[214] An impressive QE for photocatalytic CO_2 reduction has been achieved when using UV light: Inoue et al.[218] reported 32.5% QE for the reduction of CO_2 in aqueous bicarbonate to HCOOH at Cd-modified ZnS microcrystals illuminated at 280 nm; Tseng and coworkers achieved QE of 10% for photoreduction of CO_2 at sol–gel derived Cu-modified TiO_2 illuminated at 254 nm in aqueous base;[219] while Slamet et al.[220] reported photocatalytic reduction of CO_2 to CH_3OH at UV-illuminated copper oxide doped TiO_2 nanocrystals in aqueous bicarbonate with QE = 19.2%. Visible light photocatalytic CO_2 reduction is still considerably less efficient: Sato et al.[221] reported 1.9% QE for photocatalytic conversion of CO_2 to mixtures of CO, HCOOH, and H_2 at nitrogen-doped Ta_2O_5 modified with ruthenium polypyridyl cocatalysts. Typical QEs for the photocatalytic reduction of CO_2 to CH_3OH and CH_4 using visible light are even lower: ~0.02% to 0.2%.[222–224] Though the efficiencies achieved with visible light illumination are low, the high QE achieved under UV light suggests that the CO_2 reduction bottleneck in the catalytic cycle is not necessarily prohibitive to making visible light photocatalytic CO_2 reduction technologically viable. As is the case with visible light photocatalytic water splitting, the success of the CO_2 pathway will strongly depend on the right semiconductor design or sensitization scheme to efficiently produce reactive electron–hole pairs under visible illumination.

2.3.3 *Application of nanophotonics to solar fuels photocatalysis: photonic crystals for enhanced light harvesting*

Research in the past decade has demonstrated that photocatalytic materials either incorporated into or expressed directly as PCs are ~2× to 3× more active than the standard nanostructured forms of the same materials, regardless of the choice of semiconductor photocatalyst. Several illustrative examples will be specifically described below. PCs are periodic structures with alternating phases of high- and low refractive index materials in one, two, or three dimensions.[225–228] Radiation of wavelengths comparable to the PC feature dimensions is diffracted according to a modified version of Bragg's law (fitted to the geometry and refractive indices of the phases in the PC). The most strongly diffracted wavelengths cannot propagate in the PC structure; the wavelength at the center of this distribution is known as the stop band, or photonic bandgap. PCs enhance light absorption in the semiconductor via the slow photon effect. Photons with energies slightly higher and lower than the stop band are substantially slowed, with light frequencies at the low-energy (red) edge of the stop band localized and multiply scattered in the higher dielectric part of the PC; those at the high-energy (blue) edge are multiply scattered within the low-index portion.[229] In semiconductor photocatalysis, the slow photon effect enables greater interaction of the slowed photons with the semiconductor or sensitizer, improving the probability of their absorption.

The most frequently applied PC geometry in photocatalysis, depicted in Fig. 9, is the inverse opal,[230] which is relatively simple to fabricate and allows control of feature dimensions, enabling tuning of the stop band. Inverse opals are commonly synthesized by infiltrating a colloidal array of carboxylate-modified polystyrene spheres with metal oxide precursor solutions followed by subsequent removal of the colloidal array and calcination.[231–233]

2.3.4 *Hydrogen generation by photocatalysis at TiO_2 photonic crystals*

Liu et al.[235] employed a series of TiO_2 PC films modified with Pt nanoparticles with stop bands ranging from 307 to 434 nm in photocatalytic hydrogen generation experiments and observed enhancement of photocatalytic activity relative to Pt/TiO_2 control materials that were not

Downloaded From: http://photonicsforenergy.spiedigitallibrary.org/ on 01/26/2016 Terms of Use: http://spiedigitallibrary.org/ss/TermsOfUse.aspx

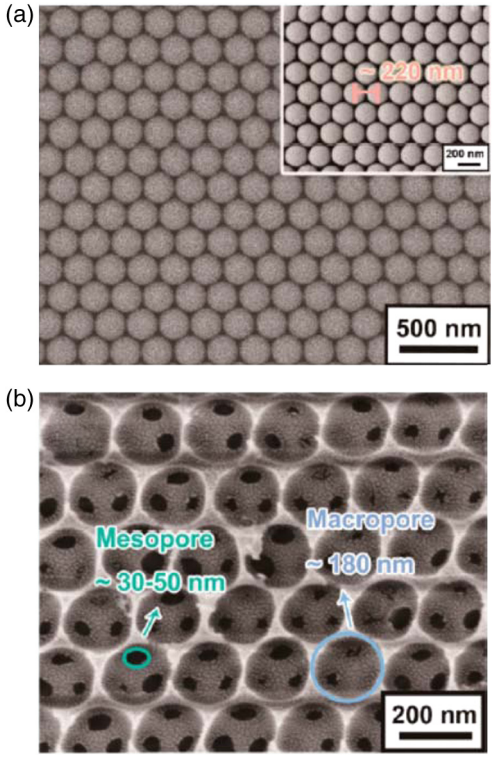

Fig. 9 SEM of (a) colloidal crystal template of polystyrene spheres (200 nm) and (b) three-dimensional ordered macromesoporous architecture of Mo:$BiVO_4$. (Reproduced with permission from Ref. 234. Copyright ACS.)

incorporated into PC structures. The largest enhancement factors (EFs) under white light illumination occurred for PC films with stop bands of 307 nm (EF = 2.4) and 342 nm (EF = 2.5). Semiconductor photocatalysts sensitized to visible light are also readily adaptable for PC-based enhancement of photocatalytic activity. For example, modification of TiO_2 with surface plasmon resonance (SPR) active gold (Au) nanoparticles has recently emerged as a viable strategy for enhancing visible light absorption.[236–239] PEC water splitting at TiO_2 PCs modified with 10-nm Au nanoparticles was enhanced by a factor of 2 relative to Au-modified nanocrystalline (but nonphotonic) TiO_2 films.[240] Alternative materials to TiO_2 for photocatalytic water splitting[194–196] also benefit from PC-enabled improvement of light utilization. The inverse opal PC design has been applied to photocatalytic iron oxides,[241] tungsten oxide,[242,243] and binary oxides.[234,244,245] Enhancement of water-splitting photocatalytic activity is consistently two to three times higher than that of the non-PC control materials.

Light-scattering structures more complex than inverse opals also enhance water-splitting photocatalysis. Because the more complex structures are imperfectly periodic or aperiodic over the length of the light scattering layer, photocatalytic enhancement derives from disorganized internal scattering of photons rather than by slow photon effects. Templated TiO_2 replicas of butterfly wings, modified with Pt nanoparticles and featuring semiordered arrays of holes and inverted ridges, enhanced photocatalytic water splitting 2.3× compared to that at nonphotonic Pt-modified TiO_2.[246] Similarly, porous TiO_2 structures templated from leaves exhibited enhanced light absorption and H_2-generation enhancement.[247]

2.4 *Optical and Photonic Sensors for Energy Harvesting and Power Production*

Optical and photonic sensors are commonplace for a wide variety of applications in the broad field of energy. In this section, their specific use in three very different applications relating to energy harvesting and the production of power will be presented, namely solar thermal and PV systems, the oil and gas industries, and wind turbines.

Downloaded From: http://photonicsforenergy.spiedigitallibrary.org/ on 01/26/2016 Terms of Use: http://spiedigitallibrary.org/ss/TermsOfUse.aspx

2.4.1 *Sun-tracking systems*

The output power of solar thermal and PV systems can be maximized by the use of sun-tracking systems, defined as electromechanical devices for orienting the solar energy systems toward the sun. Given that the diurnal and seasonal movement of the earth affects the radiation intensity on any solar energy system,[248] sun-tracking devices are used to determine with a high degree of accuracy the position of the sun throughout the course of the day on a yearly basis. As such, sun trackers are in charge of moving the solar energy systems to compensate for the motion of the earth, aiming at keeping the best orientation relative to the sun, i.e., perpendicular to solar radiation. The use of sun trackers has the potential to increase the collected energy by 10% to 100%, depending on many factors including the time of the year and the geographical position. In the particular case of concentrator applications for PVs and solar thermal applications, tracking systems are essential because concentrators do not produce energy unless pointed at the sun.

Solar tracking can be active or passive and can be implemented as one- or two-axis systems.[249] Single-axis trackers follow the sun's apparent east-to-west movement, while dual-axis trackers also tilt the solar collector or module to follow the sun's altitude angle.[250] Figure 10(a) shows schematic diagrams of the operation of single- and dual-axis tracking systems, while Fig. 10(b) illustrates a prototype of a dual-axis tracking system, comprising two stepper motors, a control circuit board and drivers, reducing gears, a sun positioning device (photodiode array), a global positioning system module, and fibers. Commercially, tracking systems are available in either a single-axis or a dual-axis design.

Active trackers can be classified as either open-loop or closed-loop types,[249] depending on their mode of signal operation. Succinctly, an open-loop type of controller computes its input into a system using only the current state and the algorithm of the system and without using feedback to determine if its input has achieved the desired goal (i.e., algorithm-based). Closed-loop types of sun-tracking systems are based on feedback control principles. In these systems, a number of inputs are transferred to a controller from sensors, which detect relevant parameters induced by the sun, manipulated in the controller and then yield outputs (i.e., sensor-based).

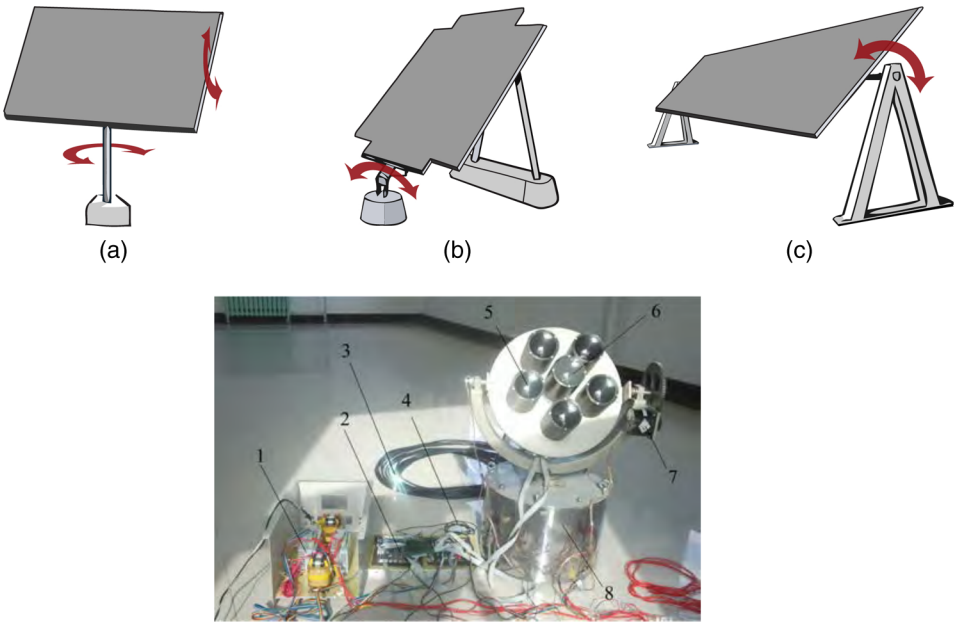

Fig. 10 Schematic diagrams of different solar trackers: (a) dual-axis tracker, (b) polar aligned single-axis tracker, and (c) horizontal single-axis tracker. (Reproduced from Ref. 251). Lower panel: Prototype of a dual-axis sun tracking system and concentrated sunlight transmission system via fibers. (Reproduced from Ref. 252.)

Downloaded From: http://photonicsforenergy.spiedigitallibrary.org/ on 01/26/2016 Terms of Use: http://spiedigitallibrary.org/ss/TermsOfUse.aspx

In the particular case of light-sensing trackers, these typically have two or more light-sensing devices configured differentially so that they output a null when receiving the same light flux. Photodiodes, photoresistors, and pyranometers are widely employed as light-sensing devices.[253] Practical requirements for these systems include accurate position/angle determination, long life, operability in remote locations and extreme environments, and wireless connectivity.

2.4.2 *Oil and gas industries*

The oil and gas industries are constantly making measurements under extreme temperatures and pressures. Additionally, development and exploitation of oil and gas resources in increasingly difficult operating environments, including deep sea water, raises many technical challenges.

Real-time, permanent wellbore and reservoir monitoring is a critical technology for assuring safety and maximizing profitability of these fields.[254] In this regard, during the past years, electronic sensors have been slowly replaced by optical sensors which perform well under these extreme conditions.[255] They are based on recent developments in fiber optic sensing technology, resulting in reliable alternatives to conventional electronic systems for permanent, downhole production and reservoir monitoring. Attractive features of optical systems for oil field applications include the fact that there is no ignition hazard, the convenience of having the complicated parts of the system at the surface, and the possibility of continuous and extended monitoring of the temperature profile.[256]

In-well fiber optic sensors are increasingly being developed and deployed in the field for measuring such parameters as temperature, pressure, flow rate, fluid phase fraction, and seismic response. In distributed temperature sensing, the fiber itself is the sensor. A pulsed laser is sent down the fiber and anti-Stokes Raman scattering is detected. The strength of the anti-Stokes signal gives temperature information, and its timing gives depth information with 1 m precision.[256] Other sensors use Bragg grating based fiber optic systems, which combine a high level of reliability, accuracy, resolution, and stability with the ability to multiplex sensors on a single fiber, enabling complex and multilateral wells to be fully instrumented with a single wellhead penetration. These systems are being installed worldwide in a variety of operating environments.

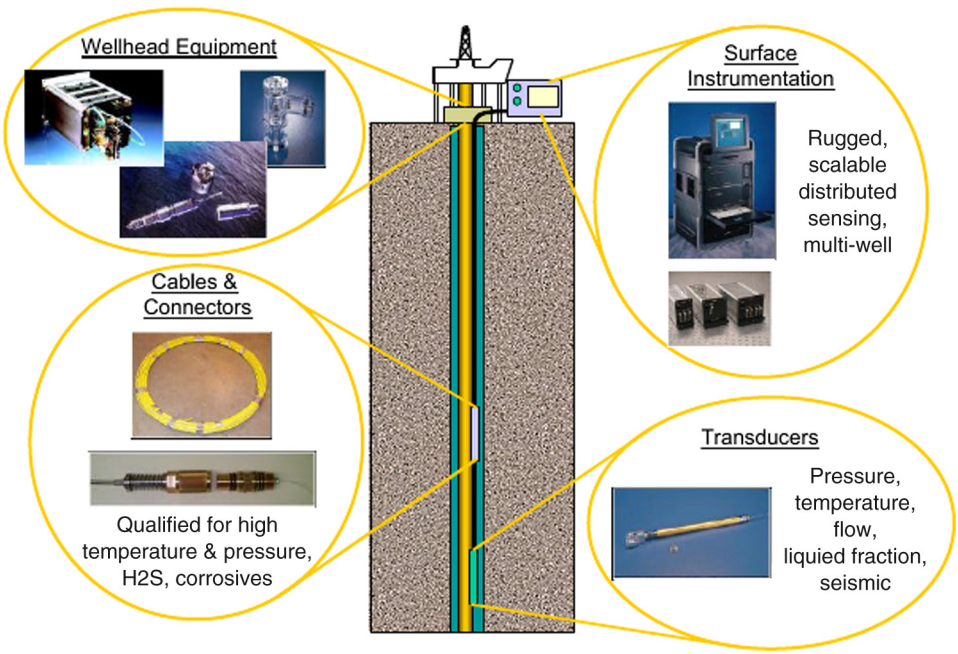

Fig. 11 Components of an in-well fiber optic monitoring system.[258]

Downloaded From: http://photonicsforenergy.spiedigitallibrary.org/ on 01/26/2016 Terms of Use: http://spiedigitallibrary.org/ss/TermsOfUse.aspx

In-well fiber optic sensing systems typically consist of four subsystems as depicted in Fig. 11: a surface instrumentation unit, wellhead outlet and surface cable, in-well cable and connectors, and transducers in the sensor assembly. The sensor assembly consists of the actual fiber optic sensors and transducers, as well as the rest of the required equipment to integrate the assembly into the production tubing string. Sensing technologies based on optical fibers have several inherent advantages that make them attractive for a wide variety of industrial applications. They are typically small in size, passive, immune to electromagnetic interference, resistant to harsh environments, and also have a capability to perform distributed sensing. These features mean that they are becoming a mainstream sensing technology.[257]

Industry tends to use fiber Bragg gratings (FBGs) to monitor reservoir pressure and temperature for a number of reasons. In particular, they are very stable sensors at high temperatures for long periods of time, electrically passive, and can be used for multiparameter sensing. FBGs are periodic perturbations that are encoded on a fiber optic core through a photo-inscription process. The perturbations allow for multipoint sensing, implying that measurements of temperature and pressure gradients can be taken by measuring the resonance shift of the FBG. These FBGs are extremely robust where studies have shown a $> 75\%$ five-year survival probability. Fiber optic based sensors can also be easily integrated into large-scale optical networks and communication systems.

2.4.3 *Light detection and ranging for wind turbines*

Light detection and ranging (LIDAR) is a technique that can determine wind speed by measuring the Doppler shift of light backscattered by aerosols (microscopic airborne particles moving with the wind) in the atmosphere.[259] It is, therefore, very useful in three ways—for surveying potential wind farm sites, optimizing their design, and for dynamic adjustments to their operation. For example, LIDAR can be used to increase the energy output from wind farms by accurately measuring wind speeds and turbulence. More accurate prediction of conditions prior to construction, as well as more optimal configuration of the turbines after construction are possible using remote sensing and modeling tools at proposed wind turbine locations.

Additionally, in an already deployed wind farm, LIDAR allows the measurement of wind conditions before they affect turbine performance. Typical commercial wind turbines operate

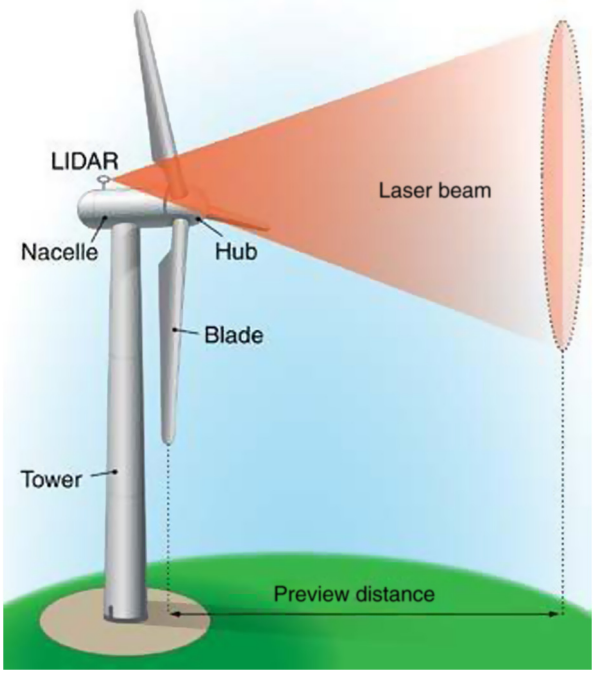

Fig. 12 Typical nacelle-based light detection and ranging measurement pattern. (Reprinted with permission of the National Renewable Energy Laboratory, from NREL publication.[260])

Downloaded From: http://photonicsforenergy.spiedigitallibrary.org/ on 01/26/2016 Terms of Use: http://spiedigitallibrary.org/ss/TermsOfUse.aspx

with variable speed and pitch controls. In below-rated wind speeds, the generator torque is controlled to extract maximum power from the wind, while the blade pitch is held constant. In above-rated wind speeds, the generator torque is held constant, while the blade pitch is used to regulate the rotational speed of the turbine using proportional-integral control. Since LIDAR systems can provide information regarding the approaching wind in advance, this allows pitch actuation to occur in advance in order to mitigate wind disturbance effects. As such, turbine control hardware can regulate the devices in order to alleviate the fatigue loading and suboptimal performance arising from anomalous wind shear, gusts, wind veer, and turbulence.[260] Accordingly, control can improve the performance and fatigue life of wind turbines by enhancing energy capture and reducing dynamic loads. Figure 12 portrays a typical LIDAR measurement system.

3 Role of Photonics in Energy Conservation

3.1 *Solid-State Lighting*

Incandescent light bulbs have served society for more than 125 years. Abundant, safe, and instantly available lighting has transformed our lives. The electromagnetic spectrum generated from the heating of the tungsten filament in an incandescent bulb primarily covers the infrared spectrum with a small portion in the visible region.[261] The result is low efficiency, but even so, these incandescent bulbs transformed lighting in the early part of the 20th century, and their importance is demonstrated by their use for over a century.

The key advances for lighting technologies in the 21st century are driven primarily by energy efficiency, color quality, and cost-effectiveness. Today, lighting accounts for ~22% of electricity energy consumption.[262] The rising cost and demand for energy result in the need for energy-efficient lighting technologies. Incandescent bulbs are limited by their relatively low-energy efficiency (~4%) and efficacy (~20 lm/W). Such limitations drive the need for innovation and new approaches for more efficient lighting, while maintaining good color rendering. The development of new electronic and photonic materials with enhanced properties, as well as advances in nanotechnology, will lead the lighting revolution in the 21st century. This cannot be accomplished without an improved understanding of the properties of both inorganic and organic semiconductors and the roles they play in device architectures.

3.1.1 *Progress in III–V and III-nitride semiconductor lighting technologies*

The areas of inorganic-based solid-state lighting were primarily driven by both III–V compounds and III-nitride compound semiconductors, specifically InAlGaP for red emitters[263] and InGaN for blue and green emitters.[264–267] Early demonstrations of practical visible emitters were based on the work by Holonyak and Bevacqua, and Allen and Grimmeiss resulting in the demonstration of ternary GaAsP-based LEDs.[8,9] The use of blue-emitting LEDs and yellow phosphors was required for enabling white LEDs. Significant roadblocks existed in the early development of InGaN and GaN-based heterostructure materials and devices for blue emission. Innovation driven by Amano et al.[264] in the growth of GaN on sapphire and the p-type doping activation in GaN by Akasaki, Amano, and Nakamura resulted in practical device technologies based on p–n diodes for lasers and LEDs.[265–267] Breakthroughs in InGaN-based blue-emitting LEDs were awarded the 2014 Nobel Prize in Physics.[6]

Following on the early work on ternary GaAsP-based materials, the fields of red LEDs shifted to InGaP/InAlGaP heterostructures for realizing practical device technologies. The early progress in InAlGaP-based LEDs was primarily implemented in display applications. The PCE of InAlGaP-based emitters was up to 50% for devices emitting at 610 nm. The key approaches resulting in high brightness red-emitting InAlGaP LEDs were the introduction of GaP transparent substrates, improved understanding in suppressing drift carrier leakage, and die-shaping for improved light extraction efficiency. The limitations of the efficiency of red-emitting InAlGaP LEDs were attributed to the intrinsic constraint in the crossover from a direct bandgap to an indirect bandgap for InAlGaP materials,[268] which in turn limits the maximum band-offset achievable in InAlGaP-InGaP heterostructures. The low band-offset achievable

Downloaded From: http://photonicsforenergy.spiedigitallibrary.org/ on 01/26/2016 Terms of Use: http://spiedigitallibrary.org/ss/TermsOfUse.aspx

in InAlGaP-InGaP increases thermally driven carrier leakage processes,[269,270] which has an impact on both the internal quantum efficiency and the current injection efficiency, in particular at high device operating temperatures.[271] Several approaches have been pursued to advance the InAlGaP technologies, specifically the development of active regions with increased spontaneous emission rate for high radiative efficiency and improved heterostructures for achieving higher current injection efficiency.

The progress in nitride-based LEDs took a relatively different route. The early demonstration of light emission in GaN was reported by Pankove et al.[272] Progress in III-nitride based semiconductors was limited by the challenges to grow them with low dislocation density, the need for growing GaN-based alloys on non-native substrates, and challenges to incorporate p-type doping in these material systems. The key developments in the early stage of InGaN-based LEDs and lasers[264–267,273,274] were driven by innovation in growth, the development of the methods to form heterostructures, the incorporation of active dopants, and the formation of devices with both p-type and n-type semiconductors. The later stage of the visible nitride-based technologies was primarily driven by the device-focus and nano-oriented innovations in InGaN-based platform for addressing the limitations to achieve high internal quantum efficiency emitting devices including lasers.[275–278] These advances in nitride semiconductor technologies have resulted in worldwide mass-scale implementation of LED technology into consumer-grade applications. Coupling with yellow phosphor, the InGaN-based LEDs resulted in white light emission with efficacy > 300 lm/W.[279]

Achieving high-efficiency and high-efficacy LEDs based on III-nitride active media is critical in ensuring their continued success and improvement in device quality for numerous technological applications. Despite impressive advances achieved in the past decade, numerous issues remain that need to be addressed.[280,281] The internal quantum efficiency of the LEDs drops significantly as the emission wavelength is extended into the green spectral regime and beyond.[275–278] The primary limitations are attributed to the charge separation issue in the quantum wells and phase separation in a high In-content InGaN alloy. Recent work using large overlap quantum well concepts aims to address the charge separation issue.[275–278] Meanwhile, wafer scale reduction in dislocation density has been achieved by GaN epitaxy on nanopatterned sapphire substrates[282–285] and has recently been implemented in industry.[286]

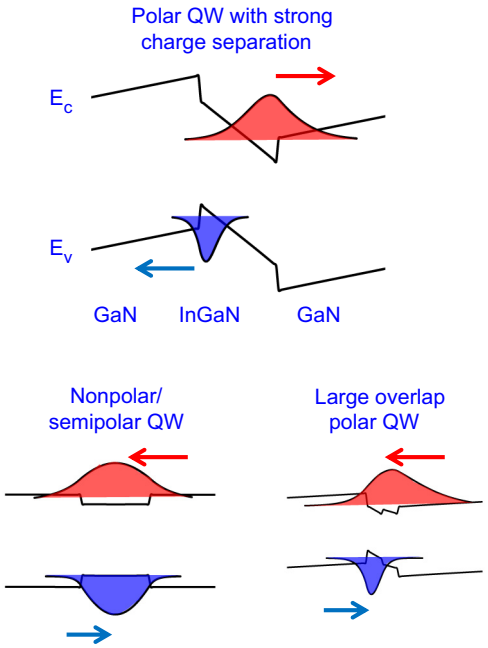

Fig. 13 A schematic diagram illustrating the charge separation issue in InGaN quantum wells, and the relevant approaches to suppress it using large overlap quantum well concept and growth along non/semipolar orientation.

Downloaded From: http://photonicsforenergy.spiedigitallibrary.org/ on 01/26/2016 Terms of Use: http://spiedigitallibrary.org/ss/TermsOfUse.aspx

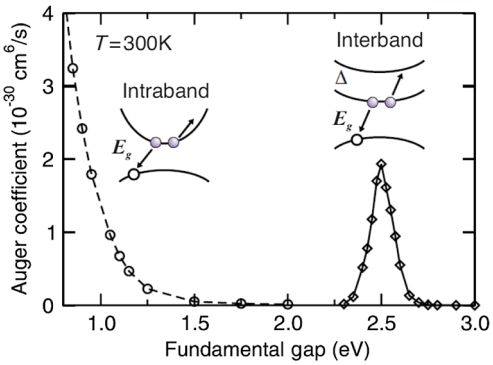

Fig. 14 The Auger coefficient for both interband and intraband processes in InGaN. The results, computed by taking into consideration materials from first principle analysis, indicate the importance of the Auger effect in InGaN. (Reproduced from Ref. 296.)

The development of efficient green/yellow and red-emitting III-nitride based emitters remains a key challenge for enabling monolithically integrated white LEDs, and these issues have been targeted using new active region designs[287–289] and growth along different facets,[290] as shown in Fig. 13. Another important issue is addressing the drop in efficiency at high current densities, known as efficiency droop, in InGaN-based LEDs. Several approaches based on new barrier designs for suppressing carrier leakage have been investigated to suppress the droop,[291–295] but complete suppression or removal of the droop requires suppression of Auger processes in the active region,[296–298] as indicated in Fig. 14. The need for a large-scale and cost-effective manufacturing process for GaN-based substrates remains the key issue for lowering the production cost of LEDs.[299] The need for a red phosphor is important for enabling improved color quality in white LEDs.[300] Scalable and cost-effective methods for achieving improved light extraction efficiency in III-nitride LEDs are also needed.[301–303]

Figure 15 illustrates the rapid improvement in the efficiency and the drop in cost for LED-based lighting technology.[304] The efficiency of both red and blue LEDs has progressed tremendously during the past 20 years. White light emission is usually produced by combining a blue LED with a phosphor. The resulting phosphor-converted white LEDs are widely used, and, as can be seen in Fig. 15, their cost ($/lumen) has fallen every year, following the trend originally made for red LEDs. This on-going development and progress in LEDs will ensure their continued success in displacing all present day lighting technologies.

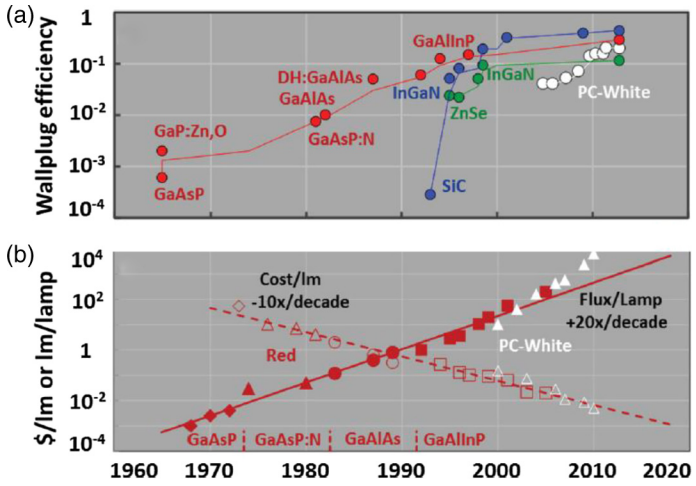

Fig. 15 Historical development of (a) wall plug efficiency of commercial red, green, blue, and phosphor-converted white light-emitting diodes (LEDs) and (b) performance (lumen/package) and cost ($/lumen) for commercial red and phosphor-converted white LEDs. (Reproduced from Ref. 304.)

Downloaded From: http://photonicsforenergy.spiedigitallibrary.org/ on 01/26/2016 Terms of Use: http://spiedigitallibrary.org/ss/TermsOfUse.aspx

3.1.2 *Progress in organic light-emitting technologies*

OLEDs were first demonstrated by Tang and Vanslyke[305] in the 1980s. Kido et al.[306] succeeded in incorporating red, green, and blue emitters in one device stack and demonstrated the first broadband white emitting OLED in the 1990s. Since spin statistics dictate that the upper bound of the internal quantum efficiency of an OLED based on fluorescent emitters is 25%, useful applications were limited to simple displays in mobile phones and cars. In the late 1990s, Baldo et al.[307] demonstrated that the limitation on the 25% upper limit of the internal quantum efficiency can be overcome with the use of phosphorescent emitters having a heavy central metal atom. Because of the strong spin–orbit coupling in these phosphorescent emitters, photons can be generated via both singlet and triplet excitons, and the internal quantum efficiency can reach 100%. Since the development of phosphorescent OLEDs, these devices have been seriously considered for solid-state lighting applications.[308,309] Today, white OLEDs with efficiencies up to 100 lm/W and color rendering indices close to 90% have been demonstrated by companies such as LG Chemical and Konica Minolta, and OLED lighting products have been introduced in the market place in the last couple years.[310,311]

White OLEDs are typically devices with multiple emitters in a device stack. As shown in Fig. 16(a), a white OLED has the following device architecture: an indium tin oxide (ITO) transparent electrode, a hole injection/transport layer, a broad band emitting layer, an electron injection/transport layer, and a top metal reflective electrode, all fabricated on a glass substrate. Metal oxides are sometimes used as charge injection layers as well as for the anode, and their use in OLEDs has recently been reviewed.[312] Individual red, green, and blue emitting layers can also be used, and the generated light is transmitted through the bottom transparent electrode and glass substrate. For lighting applications, a high luminance is required, resulting in a high operating voltage due to the low charge carrier mobilities in organic semiconductors. The high operating voltage leads to lower power efficiencies and degrades the device lifetime. To alleviate these problems, tandem stacked OLEDs were developed as shown in Fig. 16(b), which consist of two or three OLEDs connected serially with the so-called charge generation layers. In this device architecture, the charge generation layer plays a key role in connecting the individual OLEDs, and supplying electrons and holes to the adjacent connecting OLEDs. These devices behave like a multiple-photon device by having one electron going through the device stack generating multiple photons from the different emitting layers. The advantage of this device architecture is the lower overall current density through the device stack and, hence, a higher power efficiency and longer lifetime. Another advantage is that the emitting color can easily be tuned using

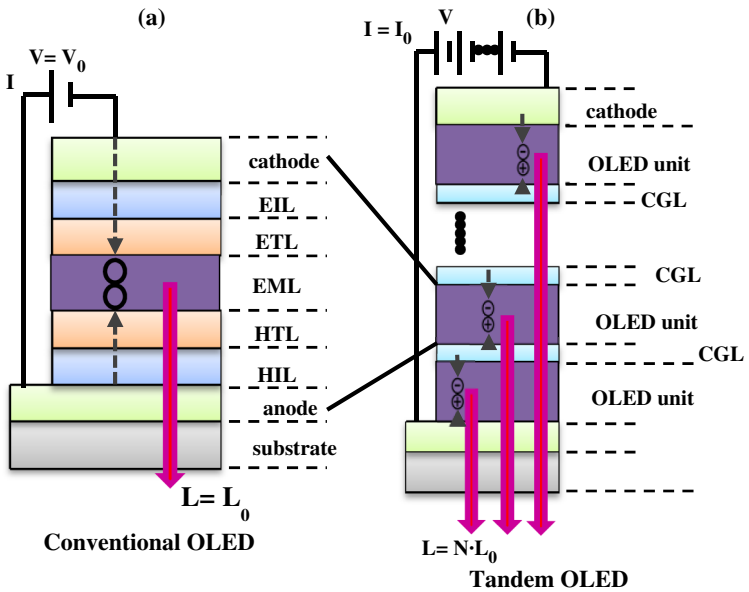

Fig. 16 Schematic drawings of (a) a conventional OLED and (b) a tandem OLED.

Downloaded From: http://photonicsforenergy.spiedigitallibrary.org/ on 01/26/2016 Terms of Use: http://spiedigitallibrary.org/ss/TermsOfUse.aspx

different red, green, and blue emitters. Using this architecture, high-performance tandem white OLEDs with high luminance efficiency (~70 lm/W) have been reported.[313]

3.2 *Flat Panel Displays*

The display of information is a major part of everyday life and the number of displays—many of them turned on for most of the day—is remarkable. They include computer monitors, televisions, and information signs in city centers, at airports and railway stations, and so on. Electronic displays have gone through several generations of technology cycles in the last 30 years. Prior to the 1990s, cathode ray tubes (CRTs) were the only form of displays used in consumer electronics. The term flat-panel displays was not in existence, and the only flat-panel displays available were electroluminescence displays, which were primarily used for military applications. The key driver for flat-panel displays was the progress made in the amorphous silicon technology. In active matrix displays, each pixel is driven with a driver circuit and large-area thin-film electronics are required. In the late 1980s, amorphous silicon PVs were seriously considered as a low-cost alternative to crystalline silicon PVs for solar energy harvesting and conversion. However, one of the main problems with amorphous silicon is that it is full of defects associated with dangling bonds. A key development was to hydrogenate amorphous silicon to reduce the number of dangling bonds,[314] and that led to the realization of amorphous silicon for PV[315] and thin-film electronic[316] applications. While amorphous silicon PV did not take off, advances made in amorphous silicon led to the commercialization of amorphous silicon thin-film transistor (TFT) technology for active matrix liquid crystal displays (TFT-LCDs).

The major challenge in TFT technology is to achieve an adequate manufacturing yield due to the very low tolerance to pixel defects. For computer displays, an LCD panel typically consists of ~1 million pixels. Because these defects are visible, only two to three dead pixels are allowed in the entire display panel, which posed a major manufacturing yield problem and led to the very high price of LCD panels. For large-screen TVs, the only viable technology was rear projection TVs. There were several versions of projection TVs. The initial light engines used for projection TVs were CRTs. During the 1990s, Texas Instruments developed the digital light processor (DLP) technology for projection TVs. DLPs are silicon chips with arrays of digital mirrors to modulate light reflection creating digital images on a screen. Another rear projection technology was liquid crystals on silicon (LCOS), where LC pixels were fabricated on a silicon chip and images were created from light reflection from the LCOS chips. While large-screen TVs can be made with projectors, they are generally very bulky and heavy with high power consumption.

The earliest flat-panel TV technology introduced to the consumer market was plasma displays. Early this century, it was the only flat-panel technology. Compared with TFT-LCDs, they were less expensive to make and offered an excellent image quality with a high speed of response for videos. As the display manufacturing base moved from Japan to South Korea and Taiwan, the cost of TFT-LCDs started to fall. LCDs slowly started replacing CRTs for computer monitors and have since largely replaced plasma TVs to become the dominant technology for flat-panel displays. Another promising technology is emerging for flat-screen TVs, which is based on using an OLED as the pixel. Figure 17 shows the historical development and progress of commercial OLED products. Compared to conventional LCDs, OLEDs offer several advantages: better color saturation, higher speed of response, and larger viewing angle. OLED dot matrix displays were first introduced by Motorola in 2000. In 2010, Samsung introduced active matrix OLED (AMOLED) displays in its Galaxy smart phones, and since then, AMOLEDs have become a main stream display technology used in smart phones and tablets. In 2014, LG introduced the first commercial OLED TVs. However, the price of OLED TVs is significantly higher than that of LCD TVs. As the cost of OLED manufacturing continues to decline, OLEDs is envisioned to be the technology of the future for TV displays.

While the technology drivers for consumer electronics are cost and performance, energy consumption is also an important factor for consumers and regulators, and has been the driving force for going from plasma TVs to LCD TVs. For example, a 55 in. plasma TV consumes ~120 W of power, while an LCD TV of the same size consumes about half as much, 60 W. In principle, OLEDs should have lower power consumption than LCDs because they are self-emissive, so that the losses in the color filters could be avoided. However, the first

Downloaded From: http://photonicsforenergy.spiedigitallibrary.org/ on 01/26/2016 Terms of Use: http://spiedigitallibrary.org/ss/TermsOfUse.aspx

Fig. 17 Historical development of commercial OLED displays.

OLED TVs actually consume more power than their LCD counterparts as shown in Fig. 18. There are two reasons for the higher power consumption. First, the pixel FF in an OLED TV is only ~20% to 30%. For an average luminance of 350 Cd/m^2, the average peak luminance at each pixel can exceed 1000 Cd/m^2. This high brightness requires a high operating voltage, resulting in a higher power consumption. Second, blue is the weakest color in OLEDs since low-efficiency blue fluorescent emitters are used in OLED displays, limiting their power efficiency. This is due to stability issues associated with the present blue phosphorescent emitters. Further progress in the synthesis of stable phosphorescent blue emitters and in pixel design will lead to an OLED TV with a better overall power efficiency and superior performance compared to that of its LCD analog.

3.3 *Light Management for Display and Lighting Applications*

Light management is an important aspect for both solid-state lighting and display applications incorporating either inorganic LEDs or OLEDs, particularly in relation to the light extraction efficiency of these devices. Although the internal quantum efficiency of the light-emitting layers used for LEDs and OLEDs can be close to 100%, the majority of the light generated is trapped inside the device. Due to the mismatch in refractive indices among air ($n = 1$), glass ($n \sim 1.5$), organic light-emitting or carrier transport layers ($n = 1.7$ to 1.9), and inorganic light-emitting or charge transport injection layers ($n = 2$ to 4), only a small fraction, ~10% to 25%, of the total of generated photons can be extracted from an LED or OLED device with planar interfaces. The rest of the photons are either trapped in guided photonic modes inside the substrate, the emitting layer(s), and the carrier injection layers, or are coupled to guided/trapped surface plasmon polariton modes at the metal electrode.[317,318] Thus, to obtain a high external quantum efficiency (EQE)

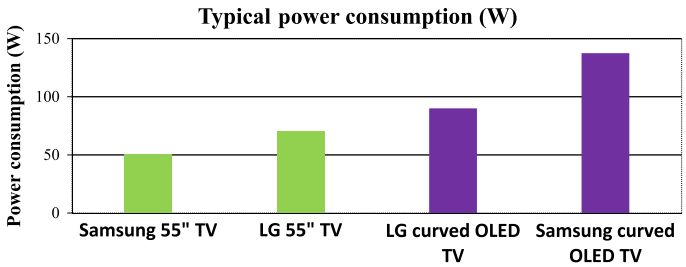

Fig. 18 Typical power consumption of liquid crystal display versus OLED TVs.

Downloaded From: http://photonicsforenergy.spiedigitallibrary.org/ on 01/26/2016 Terms of Use: http://spiedigitallibrary.org/ss/TermsOfUse.aspx

(i.e., ratio of optical output power to electrical input power), it is very important to recover the trapped photons.

For LEDs, a host of macroscale and microscale lens structures have been applied to the active light-emitting region to extract trapped photons. For OLEDs, extraction techniques, such as microlens arrays, sand-blasting, and light scattering films, have been used to extract the substrate mode, resulting in ~50% enhancement in light outcoupling efficiency.[319–321] A variety of approaches for extracting wave-guided modes trapped in ITO/organic layers, such as PCs, corrugated grating substrates, and high-index substrates, have been demonstrated to enhance the light outcoupling efficiency.[322–326] Mie scattering supported by dielectric nanostructures and localized SPRs supported by metallic nanostructures are also effective at increasing the light extraction efficiency of light-emitting devices due to their large scattering cross sections. While these techniques are effective for extracting thin-film guided modes, they have their shortcomings. For example, light emission from devices fabricated on PCs is highly dependent on the emission wavelength and emission angle, which is not suitable for broadband white light sources. High-index substrates are very effective for extracting thin-film guided modes for white light, but the high cost of high-index substrates, such as sapphire, might be prohibitive for general lighting applications. While corrugated substrates are also very effective for extracting thin-film guided modes without wavelength and emission angle dependence, the process to fabricate corrugated structures must be compatible with high volume manufacturing. Furthermore, incorporation of nanostructures can increase nonradiative recombination or degrade the electrical performance of a LED or OLED.

Various approaches to extract propagating surface plasmon polariton modes at metal electrodes in OLEDs have been reported. One approach is to eliminate the use of a metal as an electrode. Kim et al.[327] have demonstrated transparent OLEDs without using metal electrodes and obtained an EQE exceeding 60%. Another approach uses corrugated high-index substrates to fabricate OLEDs such that the corrugation is preserved at the metal–organic interface. Using this approach, EQEs greater than 50% have been obtained. Furthermore, wavelength-scale periodic microstructures have facilitated light outcoupling of surface plasmon polariton modes in dendrimer-based OLEDs.[328] While propagating surface plasmon polaritons are seen as undesirable in relation to the light extraction efficiency of both LED and OLED devices, increases in the radiative decay rate of the emitting material (to either improve the internal quantum efficiency or to facilitate faster device modulation rates) have been shown to be one beneficial effect of coupling to propagating surface plasmon polaritons.[320,329–336] For example, one of the earliest studies of the effect of surface plasmons on the emission rate of materials of interest for LEDs was carried out by Neogi et al.[334] by coupling InGaN/GaN quantum wells to surface plasmons supported by silver thin films. The spontaneous emission rate of the quantum well into the surface plasmon supported by the silver film was up to 92 times faster than that of the quantum well into free space. Both silver film thickness and the distance between the quantum well and the silver film were parameters that greatly affected the emission rate. Okamoto et al.[335] demonstrated increases in the internal quantum efficiency from InGaN quantum wells from 6 to 18 and 41% after Al and Ag film coating, respectively. The internal quantum efficiency enhancement was attributed to spontaneous emission rate increases arising from emission coupling to surface plasmon polariton modes. A 10-nm-thick GaN layer was placed between the metal films and the quantum well to optimize the efficiency enhancement.

3.4 *Optical Communications and Interconnects*

A fast means of communications over long distances has always been essential to the development and ultimate success of human societies. Often the focus of such communications has been in the areas of commerce and defense. Early societies often used smoke signals as a means of communication between major population centers. Others have used couriers, either in the form of humans or animals, such as pigeons. However, a number of societies found that the use of light was most convenient for communicating over long distances. For example, in the eighth century, a system was devised by Leo the Mathematician within the Byzantine Empire for optical communication of imperial edicts and defense-related matters using a system of lighting fixtures or

Downloaded From: http://photonicsforenergy.spiedigitallibrary.org/ on 01/26/2016 Terms of Use: http://spiedigitallibrary.org/ss/TermsOfUse.aspx

beacons that originated in the capital of Constantinople and emanated to the vast reaches of the Empire, particularly across Asia Minor/Anatolia.[337] Light has also always played a role for communication over shorter distances, such as within communities.

Over the past 150 years, one of the greatest changes to have shaped the world has been the remarkable advance of communications technology. The telegraph, followed by the telephone has enabled local, national, and intercontinental communication to occur at high speeds. Indeed, one of the first modern uses of photonics for human communications was developed by Bell and Tainter,[338] who showed a device for the transmission of sound using light, the so-called photophone. Bell and Tainter[338] were able to communicate via the photophone at distances as much as 213 m apart, with the confines of their laboratory apparently limiting further distances. More recently, advances in communications have underpinned the growth of e-mail and the Internet and the remarkable range of business and leisure activities that now depend on them. In parallel, over the past 50 years, the rapid development of computers means that the vast majority of communication is of data (rather than voice) and the amounts of data are increasing dramatically as we progress from text to audio to video and on to cloud storage. Furthermore, the rise of computing means that huge amounts of data are also communicated over short distances—between racks in data centers, between computers, between chips, and even within chips. It has been suggested that energy consumption for Internet traffic could reach 10% of the world's total consumption by 2018.[339]

The use of optics in telecommunications is well known. The amount of information that can be encoded on a wave is determined by the frequency of the wave carrying the signal. The development of communication has, therefore, involved using ever higher carrier wave frequencies, rising through the radio spectrum and beyond to optical frequencies. In addition to the very high-frequency carrier wave, a decisive advantage of optical communication has been the availability of optical fibers to carry the signal over huge distances with very low loss (0.2 dB/km).[340] Nowadays, optical fibers are also a critical component in local Internet networks, with a significant amount of high-speed Internet data communications within buildings being run by Ethernet cables using optical fibers.[341]

The implications of optical communication for power consumption are much less frequently addressed. In a simple implementation of electrical communication, the whole length of the link needs to be charged to the signal voltage. The longer the link, the higher is its capacitance, so more energy is needed to send each bit of information. In addition, the higher the frequency of communication, the greater is the power required because the line must be charged and discharged more times. As well as its energy cost, the growing capacitance with increasing length leads to a long RC (resistance times capacitance) time constant, thus severely limiting the data transmission bandwidth. These factors explain why optical communications are dominant in telecommunications. Not only has photonics enabled long-distance communication at high data rates, but it has enabled it to occur with much lower power consumption than a purely electrical implementation.

The current growth of computing has brought with it huge data centers consisting of arrays of processors and storage devices that communicate. A major challenge in computer design is to dissipate the heat generated in the processors. Hence, reducing energy consumption is not only important in itself, but also necessary to enable ever higher computer performance. What is the potential role of photonics? As explained above, optical communication has major advantages at long distances, but the implication is that electrical communication is preferable at short enough distances. Miller described the conditions that optical communications must fulfill to compete at shorter distances.[342] The emerging trend indicates that as time passes, communication bandwidths increase and so optical communication moves to shorter and shorter distances. Therefore, it is not just used between countries and cities, but also within universities and buildings, and increasingly within computer systems—e.g., to connect boards in data centers. A wide range of research is in progress to explore strategies to bring optical communication to shorter distances for chip-to-chip and ultimately intrachip communication. For example, an optical backplane using embedded polymer waveguides has been demonstrated.[343]

A major field of silicon photonics is developing, providing a way of using the established foundries for CMOS to make photonic devices.[341] Indeed, Si photonics are in full production and used extensively in the cable and Internet industry for bringing high-definition video to the

Downloaded From: http://photonicsforenergy.spiedigitallibrary.org/ on 01/26/2016 Terms of Use: http://spiedigitallibrary.org/ss/TermsOfUse.aspx

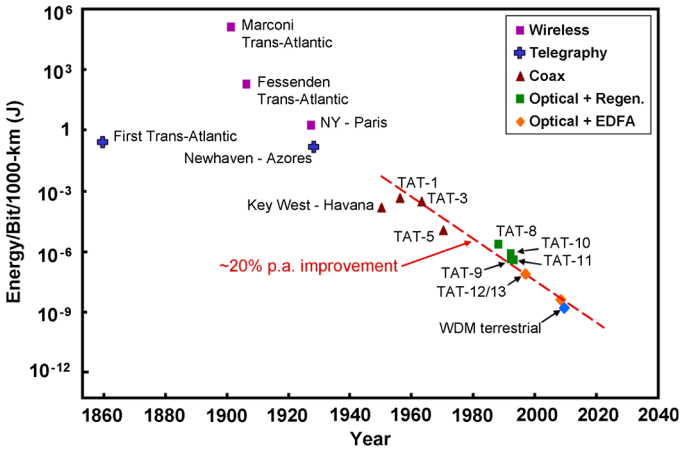

Fig. 19 Energy per bit per 1000 km of transmission distance for various transatlantic transmission systems. (Reprinted, with permission, from Ref. 347. © IEEE 2011.)

home. Companies such as Luxtera, Avago, Neophotonics, and others involved in the manufacturing of silicon photonic chips used in such communication systems are developing advanced manufacturing technologies and novel integration/packaging schemes for moving light onto chips.[344] Rapid advances are also being made on cutting-edge Si photonics based device research as well. For example, Buckwalter et al.[345] have demonstrated a silicon photonic transceiver (transmitter and receiver combined in a single unit), which gives data rates of 25 Gb/s with a bit error rate of 10^{-12}. The total power consumption is 256 mW corresponding to 7.2 pJ/bit though an external laser is also needed as silicon does not emit light. Interesting progress is being made on the limitation of Si not being an emissive material (due to its indirect bandgap). Recent research has, in fact, shown that it is possible to create light sources within silicon wafers using advances in nanophotonics. These include silicon Raman lasers with racetrack ring resonator cavities and germanium-on-silicon lasers, among other device concepts.[346] As the light source and detector are crucial components of optical communication systems, and photodetectors in silicon are readily available (as well as waveguide structures), we are moving toward an integrated photonics technology base that will allow high-speed data communications at the chip level, board level, and beyond.

The most useful metric of energy use for optical communication is J/bit.[347] The remarkable progress in improving the energy efficiency of communication systems can be clearly seen in Fig. 19. Nevertheless, considerable further savings are needed to sustain the growth of data capacity required. It is now clear that switching uses more power than transmission.[348] Again, this is a topic of extensive research. For example, Nozaki et al.[349] have demonstrated subfemtojoule all-optical switching using a PC nanocavity. The theoretical limits on optical communication have been discussed in an elegant pair of articles by Tucker.[347,348] This work suggests that there are two to three orders of magnitude of improvement on current technology possible. It would require considerable ingenuity to realize this improvement, but does suggest we can expect major progress over the coming years. Finally, while we have focused on the energy use of computing, it is important to keep in mind that ubiquitous sensing, computing, and communication enable considerable energy savings through measures such as engine management, heating controls, and smart buildings. Hence, photonics is not just enabling the information age, but enabling it in an energy-efficient way.

4 Conclusion

In celebration of the 2015 International Year of Light, this review has provided some examples of how photonics plays a crucial role in both power generation and energy conservation. Photonics is essential in the conversion of sunlight to electrical, thermal, and chemical energy. It also makes an important and significant contribution to reducing energy consumption through more efficient lighting, displays, and communications. Photonics now touches almost every area of our lives,

Downloaded From: http://photonicsforenergy.spiedigitallibrary.org/ on 01/26/2016 Terms of Use: http://spiedigitallibrary.org/ss/TermsOfUse.aspx

and its contributions to both power generation and energy conservation can be expected to grow considerably through the 21st century.

Acknowledgments

A.F.N. acknowledges support from the Fundação de Amparo a Pesquisa no Estado de São Paulo (FAPESP) and the Conselho Nacional de Desenvolvimento Científico e Tecnológico (CNPq) of Brazil. D.O'C. acknowledges support from the U.S. National Science Foundation (Grant DMR-1309459). J.J.P. acknowledges support from the U.S. Office of Naval Research. I.D.W.S. acknowledges support from the Engineering and Physical Sciences Research Council of the UK (Grants EP/K00042X and EP/L012294) and the European Research Council of the European Union (Grant 321305). N.T. acknowledges support from the U.S. National Science Foundation (Grants ECCS 1408051 and DMR 1505122).

References

1. J. C. Maxwell, "A dynamical theory of the electromagnetic field," *Philos. Trans. R. Soc. London* **155**, 459–512 (1865).
2. A. Einstein, "Über einen die Erzeugung und Verwandlung des Lichtes betreffenden heuristischen Gesichtspunkt," *Ann. Phys.* **322**(6), 132–148 (1905).
3. Nobel Media AB2014, "The Nobel Prize in Physics 1921," http://www.nobelprize.org/nobel_prizes/physics/laureates/1921/ (3 September 2015).
4. L. Piazza et al., "Simultaneous observation of the quantization and the interference pattern of a plasmonic near-field," *Nat. Commun.* **6**, 6407 (2015).
5. Nobel Media AB2014, "The Nobel Prize in Physics 2009,"http://www.nobelprize.org/nobel_prizes/physics/laureates/2009/ (22 August 2015).
6. Nobel Media AB2014, "The Nobel Prize in Physics 2014,"http://www.nobelprize.org/nobel_prizes/physics/laureates/2014/ (22 August 2015).
7. R. N. Hall et al., "Coherent light emission from GaAs junctions," *Phys. Rev. Lett.* **9**(9), 366–369 (1962).
8. N. Holonyak, Jr. and S. F. Bevacqua, "Coherent (visible) light emission from $Ga(As_{1-x}P_x)$ junctions," *Appl. Phys. Lett.* **1**, 82–83 (1962).
9. J. W. Allen and H. G. Grimmeiss, "Visible light-emitting diodes – the formative years," *Mater. Sci. Forum* **590**, 1–16 (2008).
10. H. J. Round, "A note on carborundum," *Electr. World* **49**, 309 (1907).
11. O. V. Losev, "Luminous carborundum detector and detection with crystals," Телеграфия и Телефония без Проводов **44**, 485–494; English version published as O. V. Lossev, "Luminous carborundum detector and detection with crystals," *Philos. Mag., Series 7* **6**(39), 1024–1044 (1928).
12. A. E. Becquerel, "Recherches sur les effets de la radiation chimique de la lumière solaire au moyen des courants électriques' and 'Mémoire sur les effets électriques produit sous l'influence des rayons solaires," *C. R. Acad. Sci.* **9**, 145–149, 561–567 (1839).
13. D. M. Chapin, C. S. Fuller, and G. L. Pearson, "A new silicon p-n junction photocell for converting solar radiation into electrical power," *J. Appl. Phys.* **25**, 676–677 (1954).
14. N. S. Fatemi et al., "Solar array trades between very high efficiency multi-junction and Si space solar cells," in *Proc. 28th IEEE PVSC*, pp. 1083–1086 (2000).
15. L. Tsakalakos, "Introduction to Photovoltaic Physics, Applications, and Technologies," Chapter 1 in *Nanotechnology for Photovoltaics*, CRC Press, Hoboken, New Jersey (2010).
16. W. Shockley and H. J. Queisser, "Detailed balance limit of efficiency of p-n junction solar cells," *J. Appl. Phys.* **32**, 510–519 (1961).
17. NREL, "National Center for Photovoltaics,"http://www.nrel.gov/ncpv/ (22 August 2015).
18. M. A. Green et al., "Solar cell efficiency tables (version 44)," *Prog. Photovoltaics* **22**, 701–710 (2014).
19. K. Q. Peng et al., "Synthesis of large area silicon nanowire arrays via self-assembling nanoelectrochemistry," *Adv. Mater.* **14**(16), 1164–1167 (2002).
20. A. Stoveland, "Optical modelling for photovoltaic panels," M.S. Thesis, University of Agder, Norway (2013).

Downloaded From: http://photonicsforenergy.spiedigitallibrary.org/ on 01/26/2016 Terms of Use: http://spiedigitallibrary.org/ss/TermsOfUse.aspx

21. B. M. Başol and B. McCandless, "Brief review of cadmium telluride-based photovoltaic technologies," *J. Photonics Energy* **4**(1), 040996 (2014).
22. K. Ramanathan et al., "Properties of 19.2% efficiency ZnO/CdS/CuInGaSe2 thin-film solar cells," *Prog. Photovolt* **11**, 225–230 (2003).
23. A. G. Aberle, "Thin film solar cells," *Thin Solid Films* **517**, 4706–4710 (2009).
24. O. D. Miller, E. Yablonovitch, and S. R. Kurtz, "Strong internal and external luminescence as solar cells approach the Shockley–Queisser limit," *IEEE J. Photovoltics* **2**, 303 (2012).
25. B. M. Kayes et al., "27.6% conversion efficiency, a new record for single-junction solar cells under 1 sun illumination," in *Proc. of the 37th IEEE Photovoltaic Specialists Conf.* (2011).
26. L. S. Mattos et al., "New module efficiency record: 23.5% under 1-sun illumination using thin-film single-junction GaAs solar cells," in *Proc. of the 38th IEEE Photovoltaic Specialists Conf.* (2012).
27. S. Kurtz and J. Geisz, "Multijunction solar cells for conversion of concentrated sunlight to electricity," *Opt. Express* **18**, A73–A78 (2010).
28. N. Tansu, J. Y. Yeh, and L. J. Mawst, "High-performance 1200-nm InGaAs and 1300-nm InGaAsN quantum-well lasers by metalorganic chemical vapor deposition," *IEEE J. Sel. Top. Quantum Electron.* **9**, 1220–1227 (2003).
29. L. L. Goddard et al., "Recombination, gain, band structure, efficiency, and reliability of 1.5-mu m GaInNAsSb/GaAs lasers," *J. Appl. Phys.* **97**(8), 083101 (2005).
30. J. W. Ferguson et al., *IEEE J. Quantum Electron.* **47**(6), 870–877 (2011).
31. M. Wiemer, V. Sabnis, and H. Yuen, "43.5% efficient lattice matched solar cells," *Proc. SPIE* **8108**, 810804 (2011).
32. R. Dahal et al., "InGaN/GaN multiple quantum well solar cells with long operating wavelengths," *Appl. Phys. Lett.* **94**(6), 063505 (2009).
33. M. Jamil et al., Influence of growth temperature and V/III ratio on the optical characteristics of narrow band gap (0.77 eV) InN grown on GaN/sapphire using pulsed MOVPE," *J. Cryst. Growth* **310**(23), 4947–4953 (2008).
34. T. W. Kim et al., "Properties of 'bulk' GaAsSbN/GaAs for multi-junction solar cell application: Reduction of carbon background concentration," *J. Cryst. Growth* **393**, 70–74 (2014).
35. M. Buljan et al., "Recent trends in concentrated photovoltaics concentrators' architecture," *J. Photonics Energy* **4**(1), 040995 (2014).
36. R. McConnell and M. Symko-Davies, "Multijunction photovoltaic technologies for high performance concentrators," in *Proc. IEEE 4th World. Conf. Photovolt. Energ. Conv.*, Vol. 1, pp. 733–736 (2006).
37. M. A. Green et al., "Solar cell efficiency tables," in *Proc. 20th European Photovoltaic Solar Energy Conf. (Barcelona, June)*, pp. 3 (2005).
38. E.-C. Cho et al., "Silicon quantum dot/crystalline silicon solar cells," *Nanotechnology* **19**, 245201 (2008).
39. W. G. J. H. M. van Sark et al., "Enhancing solar cell efficiency by using spectral converters," *Sol. Energy Mater. Sol. Cells* **87**, 395–409 (2005).
40. B. M. Kayes, N. S. Lewis, and H. A. Atwater, "Comparison of the device physics principles of planar and radial p-n junction nanorod solar cells," *J. Appl. Phys.* **97**, 114302 (2005).
41. L. Tsakalakos et al., "Silicon nanowire solar cells," *Appl. Phys. Lett.* **91**, 233117 (2007).
42. L. Tsakalakos et al., "High efficiency III–V micro/nano-pillar solar cells: bulk devices & growth on metal foils," in *25th European Photovoltaic Solar Energy Conf. and Exhibition/ 5th World Conf. on Photovoltaic Energy Conversion*, 6–10 September 2010, Valencia, Spain, 1CO.9.1 (2010).
43. M. Yao et al., "GaAs nanowire array solar cells with axial p-i-n Junctions," *Nano Lett.* **14**(6), 3293–3303 (2014).
44. K. Barnham et al., "Quantum well solar cells," *Appl. Surf. Sci.* **113–114**, 722–733 (1997).
45. M. Nanu, J. Schoonman, and A. Goossens, "Nanocomposite three-dimensional solar cells obtained by chemical spray deposition," *Nano Lett.* **5**, 1716 (2005).

Downloaded From: http://photonicsforenergy.spiedigitallibrary.org/ on 01/26/2016 Terms of Use: http://spiedigitallibrary.org/ss/TermsOfUse.aspx

46. P. P. Boix et al., "Current progress and future perspectives for organic/inorganic perovskite solar cells," *Mater. Today* **17**(1), 16–23 (2014).
47. J. Peng et al., "Review on life cycle assessment of energy payback and greenhouse gas emission of solar photovoltaic systems," *Renewable Sustainable Energy Rev.* **19**, 255–274 (2013).
48. S. A. McDonald et al., "Solution-processed PbS quantum dot infrared photodetectors and photovoltaics," *Nat. Mater.* **4**(2), 138–142 (2005).
49. H. Katagiri et al., "Development of CZTS-based thin film solar cells," *Thin Solid Films* **517**(7), 2455–2460 (2009).
50. S. Jeong et al., "An 8.2% efficient solution-processed $CuInSe_2$ solar cell based on multi-phase $CuInSe_2$ nanoparticles," *Energy Environ. Sci.* **5**(6), 7539–7542 (2012).
51. F. C. Krebs et al., "Upscaling of polymer solar cell fabrication using full roll-to-roll processing," *Nanoscale* **2**(6), 873–886 (2010).
52. B. O'Regan and M. Graetzel, "A low-cost high efficiency solar cell based on dye-sensitized colloidal TiO2 films," *Nature* **353**, 737 (1991).
53. Q. Yu et al., "High-efficiency dye-sensitized solar cells: the influence of lithium ions on exciton dissociation, charge recombination, and surface states," *ACS Nano* **4**(10), 6032–6038 (2010).
54. A. Yella et al., "Porphyrin-sensitized solar cells with cobalt (II/III)-based redox electrolyte exceed 12 percent efficiency," *Science* **334**, 629–634 (2011).
55. W. Zeng et al., "Efficient dye-sensitized solar cells with an organic photosensitizer featuring orderly conjugated ethylenedioxythiophene and dithienosilole blocks," *Chem. Mater.* **22**(5), 1915–1925 (2010).
56. S. Mathew et al., "Dye-sensitized solar cells with 13% efficiency achieved through the molecular engineering of porphyrin sensitizers," *Nat. Chem.* **6**(3), 242–247 (2014).
57. H. J. Snaith, "Estimating the maximum attainable efficiency in dye-sensitized solar cells," *Adv. Funct. Mater.* **20**(1), 13–19 (2010).
58. G. Hashmi et al., "Review of materials and manufacturing options for large area flexible dye solar cells," *Renewable Sustainable Energy Rev.* **15**(8), 3717–3732 (2011).
59. K. Kalyanasundaram et al., "Scale-up and product-development studies of dye-sensitized solar cell in Asia and Europe," *Dye-sensitized Solar Cells* K. Kalyanasundaram Ed., EPFL Press, Lausanne (2010).
60. J.-C. Tinguely et al., "Low-temperature roll-to-roll coating procedure of dye-sensitized solar cell photoelectrodes on flexible polymer-based substrates," *Semicond. Sci. Technol.* **26**, 045007 (2011).
61. N. S. Sariciftci et al., "Photoinduced electron transfer from a conducting polymer to buckminsterfullerene," *Science* **258**, 1474–1476 (1992).
62. Y.-J. Cheng et al., "Synthesis of conjugated polymers for organic solar cell applications," *Chem. Rev.* **109**(11), 5868–5923 (2009).
63. A. Mishra and P. Bäuerle, "Small molecule organic semiconductors on the move: promises for future solar energy technology," *Angew. Chem. Int. Ed.* **51**(9), 2020–2067 (2012).
64. X. Guo et al., "Polymer solar cells with enhanced fill factors," *Nat. Photonics* **7**(10), 825–833 (2013).
65. Z. He et al., "Enhanced power-conversion efficiency in polymer solar cells using an inverted device structure," *Nat. Photonics* **6**(9), 591–595 (2012).
66. L. Lu et al., "The role of N-doped multiwall carbon nanotubes in achieving highly efficient polymer bulk heterojunction solar cells," *Nano Lett.* **13**(6), 2365–2369 (2013).
67. Z. He et al., "Single-junction polymer solar cells with high efficiency and photovoltage," *Nat. Photonics* **9**(3), 174–179 (2015).
68. C.-C. Chen et al., "An efficient triple-junction polymer solar cell having a power conversion efficiency exceeding 11%," *Adv. Mater.* **26**(32), 5670 (2014).
69. A. K. K. Kyaw et al., "Efficient solution-processed small-molecule solar cells with inverted structure," *Adv. Mater.* **25**(17), 2397–2402 (2013).
70. J. Zhou et al., "Small molecules based on benzo[1, 2-b:4, 5-b′]dithiophene unit for high-performance solution-processed organic solar cells," *J. Am. Chem. Soc.* **134**(39), 16345–16351 (2012).

Downloaded From: http://photonicsforenergy.spiedigitallibrary.org/ on 01/26/2016 Terms of Use: http://spiedigitallibrary.org/ss/TermsOfUse.aspx

71. A. K. K. Kyaw et al., "Intensity dependence of current-voltage characteristics and recombination in high-efficiency solution-processed small-molecule solar cells," *ACS Nano* **7**(5), 4569–4577 (2013).
72. V. Gupta et al., "Barium: an efficient cathode layer for bulk-heterojunction solar cells," *Sci. Rep.* **3**, 1965 (2013).
73. Y. Sun et al., "Solution-processed small-molecule solar cells with 6.7% efficiency," *Nat. Mater.* **11**(1), 44–48 (2012).
74. Y. Liu et al., "Solution-processed small-molecule solar cells: breaking the 10% power conversion efficiency," *Sci. Rep.* **3**, 3356 (2013).
75. I. Etxebarria et al., "Polymer:fullerene solar cells: materials, processing issues, and cell layouts to reach power conversion efficiency over 10%: a review," *J. Photonics Energy* **5**(1), 057214 (2015).
76. B. Kan et al., "A series of simple oligomer-like small molecules based on oligothiophenes for solution-processed solar cells with high efficiency," *J. Am. Chem. Soc.* **137**(11), 3886–3893 (2015).
77. G. Li et al., "Polymer solar cells," *Nat. Photonics* **6**(3), 153–161 (2012).
78. S. Rajaram et al., "Effect of addition of a diblock copolymer on blend morphology and performance of poly(3-hexylthiophene):perylene diimide solar cells," *Chem. Mater.* **21**(9), 1775–1777 (2009).
79. C. H. Woo et al., "Phenyl vs alkyl polythiophene: a solar cell comparison using a vinazene derivative as acceptor," *Chem. Mater.* **22**(5), 1673–1679 (2010).
80. R. Y. C. Shin et al., "Electron-accepting conjugated materials based on 2-vinyl-4, 5-dicyanoimidazoles for application in organic electronics," *J. Org. Chem.* **74**(9), 3293–3298 (2009).
81. Y. Zhou et al., "A non-fullerene small molecule as efficient electron acceptor in organic bulk heterojunction solar cells," *Adv. Mater.* **24**(7), 957 (2012).
82. C. R. McNeill et al., "Efficient polythiophene/polyfluorene copolymer bulk heterojunction photovoltaic devices: device physics and annealing effects," *Adv. Funct. Mater.* **18**(16), 2309–2321 (2008).
83. S. Holliday et al., "A rhodanine flanked nonfullerene acceptor for solution-processed organic photovoltaics," *J. Am. Chem. Soc.* **137**(2), 898–904 (2015).
84. P. E. Schwenn et al., "A small molecule non-fullerene electron acceptor for organic solar cells," *Adv. Energy Mater.* **1**(1), 73–81 (2011).
85. E. Arici et al., "Hybrid solar cells based on nanoparticles of $CuInS_2$ in organic matrices," *Adv. Funct. Mater.* **13**(2), 165–171 (2013).
86. B. R. Saunders and M. L. Turner, "Nanoparticle-polymer photovoltaic cells," *Adv. Colloid Interface* **138**(1), 1–23 (2008).
87. S. Dayal et al., "The effect of nanoparticle shape on the photocarrier dynamics and photovoltaic device performance of poly(3-hexylthiophene):CdSe nanoparticle bulk heterojunction solar cells," *Adv. Funct. Mater.* **20**(16), 2629–2635 (2010).
88. F. S. Freitas et al., "Incorporation of nanocrystals with different dimensionalities in hybrid TiO_2/P3HT solar cells," *J. Photonics Energy* **5**, 057407 (2015).
89. P. V. Kamat, "Quantum dot solar cells. Semiconductor nanocrystals as light harvesters," *J. Phys. Chem. C* **112**(48), 18737–18753 (2008).
90. H. Lee et al., "PbS and CdS quantum dot-sensitized solid-state solar cells: old concepts, new results," *Adv. Funct. Mater.* **19**(17), 2735–2742 (2009).
91. J. N. Freitas et al., "A comprehensive review of the application of chalcogenide nanoparticles in polymer solar cells," *Nanoscale* **6**(12), 6371–6397 (2014).
92. D. Celik et al., "Performance enhancement of CdSe nanorod-polymer based hybrid solar cells utilizing a novel combination of post-synthetic nanoparticle surface treatments," *Sol. Energy Mater. Sol. Cells* **98**, 433–440 (2012).
93. M. Nam et al., "Broadband-absorbing hybrid solar cells with efficiency greater than 3% based on a bulk heterojunction of PbS quantum dots and a low-bandgap polymer," *J. Mater. Chem. A* **2**(11), 3978–3985 (2014).
94. X. Li et al., "Improved efficiency of smooth and aligned single walled carbon nanotube/silicon hybrid solar cells," *Energy Environ. Sci.* **6**(3), 879–887 (2013).

Downloaded From: http://photonicsforenergy.spiedigitallibrary.org/ on 01/26/2016 Terms of Use: http://spiedigitallibrary.org/ss/TermsOfUse.aspx

95. F. S. Freitas et al., "Hybrid silicon/P3HT solar cells based on an interfacial modification with a molecular thiophene layer," *Phys. Status Solidi A* **211**(11), 2657–2661 (2014).
96. H. J. Snaith, "Perovskites: the emergence of a new era for low-cost, high-efficiency solar cells," *J. Phys. Chem. Lett.* **4**(21), 3623–3630 (2013).
97. H.-S. Kim et al., "Organolead halide perovskite: new horizons in solar cell research," *J. Phys. Chem. C* **118**(11), 5615–5625 (2014).
98. A. Kojima et al., "Organometal halide perovskite as visible-light sensitizers for photovoltaic cells," *J. Am. Chem. Soc.* **131**, 6050–6051 (2009).
99. H. S. Kim et al., "Lead iodide perovskite sensitized all-solid-state submicron thin film mesoscopic solar cell with efficiency exceeding 9%," *Sci. Rep.* **2**, 591 (2012).
100. M. M. Lee et al., "Efficient hybrid solar cells based on meso-superstructured organometal halide perovskites," *Science* **338**, 643–647 (2012).
101. J. H. Noh et al., "Chemical management for colorful, efficient, and stable inorganic-organic hybrid nanostructured solar cells," *Nano Lett.* **13**(4), 1764–1769 (2013).
102. J. M. Ball et al., "Low-temperature processed meso-superstructured to thin-film perovskite solar cells," *Energy Environ. Sci.* **6**(6), 1739–1743 (2013).
103. J. H. Grätzel et al., "Efficient inorganic–organic hybrid heterojunction solar cells containing perovskite compound and polymeric hole conductors," *Nat. Photonics* **7**, 486–491 (2013).
104. H.-S. Kim et al., "High efficiency solid-state sensitized solar cell-based on submicrometer rutile TiO_2 nanorod and $CH_3NH_3PbI_3$ perovskite sensitizer," *Nano Lett.* **13**(6), 2412–2417 (2013).
105. N.-G. Park, "Organometal perovskite light absorbers toward a 20% efficiency low-cost solid-state mesoscopic solar cell," *J. Phys. Chem. Lett.* **4**(15), 2423–2429 (2013).
106. C.-C. Chen et al., "One-step, low-temperature deposited perovskite solar cell utilizing small molecule additive," *J. Photonics Energy* **5**(1), 057405 (2015).
107. J. Burschka et al., "Sequential deposition as a route to high-performance perovskite-sensitized solar cells," *Nature* **499**, 316–319 (2013).
108. M. Liu et al., "Efficient planar heterojunction perovskite solar cells by vapour deposition," *Nature* **501**, 395–398 (2013).
109. N. J. Jeon et al., "Solvent engineering for high-performance inorganic–organic hybrid perovskite solar cells," *Nat. Mater.* **13**(9), 897–903 (2014).
110. W. Nie et al., "High-efficiency solution-processed perovskite solar cells with millimeter-scale grains," *Science* **347**, 522–525 (2015).
111. N. J. Jeon et al., "Compositional engineering of perovskite materials for high-performance solar cells," *Nature* **517**, 476–480 (2015).
112. D. Liu et al., "Compact layer free perovskite solar cells with 13.5% efficiency," *J. Am. Chem. Soc.* **136**(49), 17116–17122 (2014).
113. S. Aharon et al., "Depletion region effect of highly efficient hole conductor free $CH_3NH_3PbI_3$ perovskite solar cells," *Phys. Chem. Chem. Phys.* **16**(22), 10512–10518 (2014).
114. W. Ke et al., "Efficient hole-blocking layer-free planar halide perovskite thin-film solar cells," *Nat. Commun.* **6**, 6700 (2015).
115. H. S. Jung and N.-G. Park, "Perovskite solar cells: from materials to devices," *Small* **11**(1), 10–25 (2015).
116. S. D. Stranks et al., "Electron–hole diffusion lengths exceeding 1 micrometer in an organometal trihalide perovskite absorber," *Science* **342**, 341–344 (2013).
117. G. Xing et al., "Long-range balanced electron- and hole-transport lengths in organic–inorganic $CH_3NH_3PbI_3$," *Science* **342**, 344–347 (2013).
118. A. H. Ip et al., "Hybrid passivated colloidal quantum dot solids," *Nat. Nanotechnol.* **7**(9), 577–582 (2012).
119. J. M. Luther et al., "Schottky solar cells based on colloidal nanocrystal films," *Nano Lett.* **8**(10), 3488–3492 (2008).
120. C. Piliego et al., "5.2% efficient PbS nanocrystal Schottky solar cells," *Energy Environ. Sci.* **6**(10), 3054–3059 (2013).
121. J. Tang et al., "Colloidal-quantum-dot photovoltaics using atomic-ligand passivation," *Nat. Mater.* **10**(10), 765–771 (2011).

Downloaded From: http://photonicsforenergy.spiedigitallibrary.org/ on 01/26/2016 Terms of Use: http://spiedigitallibrary.org/ss/TermsOfUse.aspx

122. E. H. Sargent, "Colloidal quantum dot solar cells," *Nat. Photonics* **6**(3), 133–135 (2012).
123. H. McDaniel et al., "Engineered $CuInSe_xS_{2-x}$ quantum dots for sensitized solar cells," *J. Phys. Chem. Lett.* **4**(3), 355–361 (2013).
124. P. Maraghechi et al., "The donor-supply electrode enhances performance in colloidal quantum dot solar cells," *ACS Nano* **7**(7), 6111–6116 (2013).
125. P. M. Amirtharaj and D. G. Seiler, "Optical properties of semiconductors," Chapter 36 in *Handbook of Optics*, M. Bass, Eds., 2nd ed., Optical Society of America, Washington, DC (1995).
126. K. R. McIntosh et al., "An optical comparison of silicone and EVA encapsulants for conventional silicon PV modules: a ray-tracing study," in *Photovoltaic Specialists Conf. PVSC 2009 34th IEEE*, pp. 000544–000549 (2009).
127. H. K. Raut et al., "Anti-reflective coatings: a critical, in-depth review," *Energy Environ. Sci.* **4**, 3779–3804 (2011).
128. J. Wohlgemuth et al., "Crystalline silicon photovoltaic modules with anti-reflective coated glass," in *Conf. Record of the Thirty-First IEEE Photovoltaic Specialists Conf. 2005*, pp. 1015–1018 (2005).
129. D. L. King, W. E. Boyson, and J. A. Kratochvil, "Analysis of factors influencing the annual energy production of photovoltaic systems," in *Conf. Record of the Twenty-Ninth IEEE Photovoltaic Specialists Conf.* 2002pp. 1356–1361.
130. L. Tsakalakos et al., "Strong broadband optical absorption in silicon nanowire films," *J. Nanophotonics* **1**, 013552 (2007).
131. S. Boden and D. Bagnall, "Optimization of moth-eye antireflection schemes for silicon solar cells," *Prog. Photovoltaics* **18**(3), 195–203 (2010).
132. Y. A. Xi et al., "Nanostructured anti-reflection coatings and associated methods and devices," U.S. 20100259823 A1 (2010).
133. L. Tsakalakos et al., "Nanostructured functional coatings and devices," U.S. Patent 8,933,526 (2015).
134. T. Trupke, M. A. Green, and P. Würfel, "Improving solar cell efficiencies by down-conversion of high-energy photons," *J. Appl. Phys.* **92**, 1668–1674 (2002).
135. T. Trupke, M. A. Green, and P. Würfel, "Improving solar cell efficiencies by up-conversion of sub-band-gap light," *J. Appl. Phys.* **92**, 4117–4122 (2002).
136. W. G. J. H. M. van Sark et al., "Enhancing solar cell efficiency by using spectral converters," *Sol. Energy Mater. Sol. Cells* **87**, 395–409 (2005).
137. P. Campbell and M. A. Green, "Light trapping properties of pyramidally textured surfaces," *J. Appl. Phys.* **62**, 243–249 (1987).
138. Z. F. Yu, A. Raman, and S. H. Fan, "Fundamental limit of nanophotonic light trapping in solar cells," *Proc. Natl. Acad. Sci. U. S. A.* **107**, 17491–17496 (2010).
139. E. Yablonovitch and G. D. Cody, "Intensity enhancement in textured optical sheets for solar-cells," *IEEE Trans. Electron Devices* **29**, 300–305 (1982).
140. H. R. Stuart and D. G. Hall, "Thermodynamic limit to light trapping in thin planar structures," *J. Opt. Soc. Am.* **14**, 3001–3008 (1997).
141. D. M. Callahan, J. N. Munday, and H. A. Atwater, "Solar cell light trapping beyond the ray optic limit," *Nano Lett.* **12**, 214–218 (2012).
142. J. L. Balenzategui and A. Marti, "Detailed modelling of photon recycling: application to GaAs solar cells," *Sol. Energy Mater. Sol. Cells* **90**, 1068–1088 (2006).
143. E. D. Kosten, B. M. Kayes, and H. A. Atwater, "Experimental demonstration of enhanced photon recycling in angle-restricted GaAs solar cells," *Energy Environ. Sci.* **7**, 1907–1912 (2014).
144. C. E. Petoukhoff et al., "Plasmonic electrodes for bulk-heterojunction organic photovoltaics: a review," *J. Photonics Energy* **5**(1), 057002 (2015).
145. S. Pillai et al., "Surface plasmon enhanced silicon solar cells," *J. Appl. Phys.* **101**, 093105 (2007).
146. D. M. Schaadt, B. Feng, and E. T. Yu, "Enhanced semiconductor optical absorption via surface plasmon excitation in metal nanoparticles," *Appl. Phys. Lett.* **86**, 063106 (2005).
147. H. R. Stuart and D. G. Hall, "Island size effects in nanoparticle-enhanced photodetectors," *Appl. Phys. Lett.* **73**, 3815–3817 (1998).

Downloaded From: http://photonicsforenergy.spiedigitallibrary.org/ on 01/26/2016 Terms of Use: http://spiedigitallibrary.org/ss/TermsOfUse.aspx

148. V. E. Ferry et al., "Plasmonic nanostructure design for efficient light coupling into solar cells," *Nano Lett.* **8**, 4391–4397 (2008).
149. A. Mohammadi, V. Sandoghdar, and M. Agio, "Gold nanorods and nanospheroids for enhancing spontaneous emission," *New J. Phys.* **10**, 105015 (2008).
150. Y. A. Akimov, W. S. Koh, and K. Ostrikov, "Enhancement of optical absorption in thin-film solar cells through the excitation of higher-order nanoparticle plasmon modes," *Opt. Express* **17**, 10195–10205 (2009).
151. H. A. Atwater and A. Polman, "Plasmonics for improved photovoltaic devices," *Nat. Mater.* **9**, 865–865 (2010).
152. M. W. Knight et al., "Photodetection with active optical antennas," *Science* **332**, 702–704 (2011).
153. B. Zeng et al., "Polymeric photovoltaics with various metallic plasmonic nanostructures," *J. Appl. Phys.* **113**, 063109 (2013).
154. Q. Gan, F. J. Bartoli, and Z. H. Kafafi, "Plasmonic-enhanced organic photovoltaics: breaking the 10% efficiency barrier," *Adv. Mater.* **25**, 2385 (2013).
155. K. Liu et al., "Super absorption of ultra-thin organic photovoltaic films," *Invited Paper Opt. Commun.* **314**, 48 (2014).
156. B. Zeng, Z. H. Kafafi, and F. J. Bartoli, "Transparent electrodes based on two-dimension Ag nanogrids and double one-dimensional Ag nanogratings for organic photovoltaics," *J. Photonics Energy* **5**(1), 057005 (2015).
157. W. Gaynor, J. Y. Lee, and P. Peumans, "Fully solution-processed inverted polymer solar cells with laminated nanowire electrodes," *ACS Nano* **4**, 30–34 (2010).
158. X. H. Li et al., "Polarization-independent efficiency enhancement of organic solar cells by using 3-dimensional plasmonic electrode," *Appl. Phys. Lett.* **102**, 153304 (2013).
159. P. Lalanne et al., "A microscopic view of the electromagnetic properties of sub-lambda metallic surfaces," *Surf. Sci. Rep.* **64**, 453–469 (2009).
160. W. Bai et al., "Broadband short-range surface plasmon structures for absorption enhancement in organic photovoltaics," *Opt. Express* **18**(104), A620 (2010).
161. W. Bai et al., "Double plasmonic nanostructure design for broadband absorption enhancement in organic photovoltaics," *J. Photonics Energy* **1**, 011121 (2011).
162. F. M. Wang and N. A. Melosh, "Plasmonic energy collection through hot carrier extraction," *Nano Lett.* **11**, 5426–5430 (2011).
163. S. Mubeen et al., "Plasmonic photosensitization of a wide band gap semiconductor: converting plasmons to charge carriers," *Nano Lett.* **11**, 5548–5552 (2011).
164. I. Thomann et al., "Plasmon enhanced solar-to-fuel energy conversion," *Nano Lett.* **11**, 3440–3446 (2011).
165. A. Aubry et al., "Plasmonic light-harvesting devices over the whole visible spectrum," *Nano Lett.* **10**, 2574–2579 (2010).
166. K. Aydin et al., "Broadband polarization-independent resonant light absorption using ultrathin plasmonic super absorbers," *Nat. Commun.* **2**, 517 (2011).
167. E. A. Fletcher, "Solar thermal processing: a review," *J. Sol. Energy Eng.* **123**(2), 63 (2001).
168. "Concentrating Solar Power" (PDF), pp. 11, International Renewable Energy Agency, http://www.irena.org/DocumentDownloads/Publications/RE_Technologies_Cost_Analysis-CSP.pdf (2012).
169. K. Mizuno et al., "A black body absorber from vertically aligned single-walled carbon nanotubes," *Proc. Natl. Acad. Sci. U. S. A.* **106**(15), 6044–6047 (2009).
170. M. M. Meyers et al., "High efficiency solar thermal receiver," U.S. 20110185728A1 (2011).
171. J. B. Chou et al., "Enabling ideal selective solar absorption with 2D metallic dielectric photonic crystals," *Adv. Mater.* **26**, 8041–8045 (2014).
172. Sargent & Lundy LLC Consulting Group, "Assessment of parabolic trough and power tower solar technology cost and performance forecasts," National Renewable Energy Laboratory, Sub-Contractor Report 550-34440 (2003).
173. S. Basu, Y. B. Chen, and Z. M. Zhang, "Microscale radiation in thermophotovoltaic devices—a review," *Int. J. Energy Res.* **31**, 689–716 (2007).
174. M. W. Dashiell et al., "Quaternary InGaAsSb Thermophotovoltaic Diodes," *IEEE Trans. Electr. Dev.* **53**, 2879–2891 (2006).

Downloaded From: http://photonicsforenergy.spiedigitallibrary.org/ on 01/26/2016 Terms of Use: http://spiedigitallibrary.org/ss/TermsOfUse.aspx

175. C. Ferrari et al., "Overview and status of thermophotovoltaic systems," *Energy Proc.* **45**, 160–169 (2014).
176. J. G. Kim et al., "Room-temperature 2.5 μm InGaAsSb/AlGaAsSb diode lasers emitting 1W continuous waves," *Appl. Phys. Lett.* **81**(17), 3146 (2002).
177. N. Tansu and L. J. Mawst, "Design analysis of 1550-nm GaAsSb-(In)GaAsN type-II quantum well laser active regions," *IEEE J. Quantum Electron.* **39**(10), 1205–1210 (2003).
178. I. Vurgaftman et al., "(In)GaAsN-GaAsSb type-II 'W' quantum-well lasers for emission at ($\lambda = 1.55$ μm)," *Appl. Phys. Lett.* **83**(194), 2742–2744 (2003).
179. I. Vurgaftman et al., "InP-based dilute-nitride mid-infrared type-II 'W' quantum-well lasers," *J. Appl. Phys.* **96**(8), 4653–4655 (2004).
180. D. B. Jackrel et al., "Dilute nitride GaInNAs and GaInNAsSb solar cells by molecular beam epitaxy," *J. Appl. Phys.* **101**(11), 114916 (2007).
181. T. W. Kim, T. F. Kuech, and L. J. Mawst, "Impact of growth temperature and substrate orientation on dilute-nitride-antimonide materials grown by MOVPE for multi-junction solar cell application," *J. Cryst. Growth* **405**, 87–91 (2014).
182. Y. Nam et al., "Solar thermophotovoltaic energy conversion systems with two-dimensional tantalum photonic crystal absorbers and emitters," *Sol. Energy Mater. Sol. Cells* **122**, 287–296 (2014).
183. C. Ungaro, S. K. Gray, and M. C. Gupta, "Graded-index structures for high-efficiency solar thermophotovoltaic emitting surfaces," *Opt. Lett.* **39**(18), 5259–5262 (2014).
184. G. Chen et al., "Recent developments in thermoelectric materials," *Int. Mater. Rev.* **48**(1), 45–66 (2003).
185. M. S. Dresselhaus et al., "New directions for low-dimensional thermoelectric materials," *Adv. Mater.* **19**(8), 1043–1053 (2007).
186. A. J. Minnich et al., "Bulk nanostructured thermoelectric materials: current research and future prospects," *Energy Environ. Sci.* **2**, 466–479 (2009).
187. G. Joshi et al., "Enhanced thermoelectric figure-of-merit in nanostructured p-type silicon germanium bulk alloys," *Nano Lett.* **8**(12), 4670–4674 (2008).
188. H. Tong et al., "Thermoelectric properties of lattice-matched AlInN alloy grown by metal-organic chemical vapor deposition," *Appl. Phys. Lett.* **97**(11), 112105 (2010).
189. J. Zhang et al., "High-temperature characteristics of Seebeck coefficients for AlInN alloys grown by metalorganic vapor phase epitaxy," *J. Appl. Phys.* **110**(4), 043710 (2011).
190. A. Fujishima and K. Honda, "Electrochemical photolysis of water at a semiconductor electrode," *Nature* **238**(5358), 37–38 (1972).
191. M. Anpo and M. Takeuchi, "The design and development of highly reactive titanium dioxide photocatalysts operating under visible light irradiation," *J. Catal.* **216**(1–2), 505–516 (2003).
192. S. Banerjee et al., "New insights into the mechanism of visible light photocatalysis," *J. Phys. Chem. Lett.* **5**(15), 2543–2554 (2014).
193. H. Xu et al., "Recent advances in TiO_2-based photocatalysis," *J. Mater. Chem. A* **2**(32), 12642–12661 (2014).
194. R. Abe, "Recent progress on photocatalytic and photoelectrochemical water splitting under visible light," *J. Photochem. Photobiol. C* **11**(4), 179–209 (2010).
195. A. Kudo and Y. Miseki, "Heterogeneous photocatalyst materials for water splitting," *Chem. Soc. Rev.* **38**(1), 253–278 (2009).
196. M. Hernández-Alonso et al., "Development of alternative photocatalysts to TiO_2: challenges and opportunities," *Energy Environ. Sci.* **2**(12), 1231–1257 (2009).
197. X. Chen et al., "Semiconductor-based photocatalytic hydrogen generation," *Chem. Rev.* **110**(11), 6503–6570 (2010).
198. D. Y. C. Leung et al., "Hydrogen production over titania-based photocatalysts," *ChemSusChem* **3**(6), 681–694 (2010).
199. M. G. Walter et al., "Solar water splitting cells," *Chem. Rev.* **110**(11), 6446–6473 (2010).
200. Y. Tachibana, L. Vayssieres, and J. R. Durrant, "Artificial photosynthesis for solar water-splitting," *Nat. Photonics* **6**(8), 511–518 (2012).
201. Á. Valdés et al., "Solar hydrogen production with semiconductor metal oxides: new directions in experiment and theory," *Phys. Chem. Chem. Phys.* **14**(1), 49–40 (2012).

Downloaded From: http://photonicsforenergy.spiedigitallibrary.org/ on 01/26/2016 Terms of Use: http://spiedigitallibrary.org/ss/TermsOfUse.aspx

202. Z. Li et al., "Photoelectrochemical cells for solar hydrogen production: current state of promising photoelectrodes, methods to improve their properties, and outlook," *Energy Environ. Sci.* **6**(2), 347–370 (2013).
203. F. Osterloh, "Inorganic nanostructures for photoelectrochemical and photocatalytic water splitting," *Chem. Soc. Rev.* **42**(6), 2294–2320 (2013).
204. J. Gan, X. Lu, and Y. Tong, "Towards highly efficient photoanodes: boosting sunlight-driven semiconductor nanomaterials for water oxidation," *Nanoscale* **6**(13), 7142–7154 (2014).
205. A. A. Ismail and D. W. Bahnemann, "Photochemical splitting of water for hydrogen production by photocatalysis: a review," *Sol. Energy Mater. Sol. Cells* **128**, 85–101 (2014).
206. K. Maeda et al., "Photocatalyst releasing hydrogen from water-enhancing catalytic performance holds promise for hydrogen production by water splitting in sunlight," *Nature* **440**(7082), 295 (2006).
207. Y. Lee et al., "Zinc germanium oxynitride as a photocatalyst for overall water splitting under visible light," *J. Phys. Chem. C* **111**(2), 1042–1048 (2007).
208. O. Khaselev and J. A. Turner, "A monolithic photovoltaic–photoelectrochemical device for hydrogen production via water splitting," *Science* **280**(5632), 425–427 (1998).
209. R. E. Rocheleau, E. L. Miller, and A. Misra, "High-efficiency photoelectrochemical hydrogen production using multijunction amorphous silicon photoelectrodes," *Energy Fuels* **12**(1), 3–10 (1998).
210. C. R. Cox et al., "Ten-percent solar-to-fuel conversion with nonprecious materials," *Proc. Natl. Acad. Sci. U. S. A.* **111**(39), 14057–14061 (2014).
211. D. G. Nocera, "The artificial leaf," *Acc. Chem. Res.* **45**(5), 767–776 (2012).
212. A. Dhakshinamoorthy et al., "Photocatallytic CO_2 reduction by TiO_2 and related titanium containing solids," *Energy. Environ. Sci.* **5**(11), 9217–9233 (2012).
213. E. V. Kondratenko et al., "Status and perspectives of CO_2 conversion into fuels and chemicals by catalytic, photocatalytic and electrocatalytic processes," *Energy Environ. Sci.* **6**(11), 3112–3135 (2013).
214. S. Navalón et al., "Photocatalytic CO_2 reduction using non-titanium metal oxides and sulfides," *ChemSusChem* **6**(4), 562–577 (2013).
215. S. Das and W. M. A. Wan Daud, "A review on advances in photocatalysts towards CO_2 conversion," *RSC Adv.* **4**(40), 20856–20893 (2014).
216. S. V. Habisreutinger, L. Schmidt-Mende, and J. K. Stolarczyk, "Photocatalytic reduction of CO_2 on TiO_2 and other semiconductors," *Angew. Chem. Int. Ed.* **52**(29), 7372–7378 (2013).
217. W. Tu, Y. Zhou, and Z. Zou, "Photocatalytic conversion of CO_2 into renewable hydrocarbon fuels: state-of-the-art accomplishment, challenges, and prospects," *Adv. Mater.* **26**(27), 4607–4626 (2014).
218. H. Inoue et al., "Photoreduction of carbon dioxide using chalcogenide semiconductor microcrystals," *J. Photochem. Photobiol. A* **86**(1–3), 191–196 (1995).
219. I. H. Tseng et al., "Photoreduction of CO_2 using sol-gel derived titania and titania-supported copper catalysts," *Appl. Catal. B* **37**(1), 37–48 (2002).
220. Slamet et al., "Photocatalytic reduction of CO_2 on copper-doped titania catalysts prepared by improved-impregnation method," *Catal. Commun.* **6**(5), 313–319 (2005).
221. S. Sato et al., "Visible-light-induced selective CO_2 reduction utilizing a ruthenium complex electrocatalyst linked to a p-type nitrogen-doped Ta_2O_5 semiconductor," *Angew. Chem. Int. Ed. Eng.* **49**(30), 5101–5105 (2010).
222. K. Xie et al., "Self-doped $SrTiO_{3-\delta}$ photocatalyst with enhanced activity for artificial photosynthesis under visible light," *Energy Environ. Sci.* **4**(10), 4211–4219 (2011).
223. Q. D. Truong et al., "Synthesis of TiO_2 nanoparticles using novel titanium oxalate complex towards visible light-driven photocatalytic reduction of CO_2 to CH_3OH," *Appl. Catal. A* **437**, 28–35 (2012).
224. Q. Liu et al., "Zn_2GeO_4 crystal splitting toward sheaf-like, hyperbranched nanostructures and photocatalytic reduction of CO_2 into CH_4 under visible light after nitridation," *J. Mater. Chem.* **22**(5), 2033–2038 (2012).
225. J. D. Joannopoulos, P. R. Villeneuve, and S. Fan, "Photonic crystals: putting a new twist on light," *Nature* **386**(6621), 143–149 (1997).

Downloaded From: http://photonicsforenergy.spiedigitallibrary.org/ on 01/26/2016 Terms of Use: http://spiedigitallibrary.org/ss/TermsOfUse.aspx

226. Y. N. Xia et al., "Monodispersed colloidal spheres: old materials with new applications," *Adv. Mater.* **12**(10), 693–713 (2000).
227. C. López, "Materials aspects of photonic crystals," *Adv. Mater.* **15**(20), 1670–1704 (2003).
228. K. Busch et al., "Periodic nanostructures for photonics," *Phys. Rep.* **444**(3–6), 101–202 (2007).
229. A. Imhof et al., "Large dispersive effects near the band edges of photonic crystals," *Phys. Rev. Lett.* **83**(15), 2942–2945 (1999).
230. A. Stein, B. J. Wilson, and S. G. Rudisill, "Design and functionality of colloidal-crystal-templated materials—chemical applications of inverse opals," *Chem. Soc. Rev.* **42**(7), 2763–2803 (2013).
231. S. Nishimura et al., "Fabrication technique for filling-factor tunable titanium colloidal crystal replicas," *Appl. Phys. Lett.* **81**(24), 4532–4534 (2002).
232. S. Nishimura et al., "Standing wave enhancement of red absorbance and photocurrent in dye-sensitized titanium dioxide photoelectrodes coupled to photonic crystals," *J. Am. Chem. Soc.* **125**(20), 6306–6310 (2003).
233. L. I. Halaoui, N. Abrams, and T. E. Mallouk, "Increasing the conversion efficiency of dye-sensitized TiO_2 photoelectrochemical cells by coupling to photonic crystals," *J. Phys. Chem. B* **109**(13), 6334–6342 (2005).
234. M. Zhou et al., "Photoelectrodes based upon Mo:$BiVO_4$ inverse opals for photoelectrochemical water splitting," *ACS Nano* **8**(7), 7088–7098 (2014).
235. J. Liu et al., "Enhancement of photochemical hydrogen evolution of Pt-loaded hierarchical titania photonic crystals," *Energy Environ. Sci.* **3**(10), 1503–1506 (2010).
236. Z. Liu et al., "Plasmon resonant enhancement of photocatalytic water splitting under visible illumination," *Nano Lett.* **11**(3), 1111–1116 (2011).
237. C. S. Silva et al., "Influence of excitation wavelength (UV or visible light) on the photocatalytic activity of titania containing gold nanoparticles for the generation of hydrogen or oxygen from water," *J. Am. Chem. Soc.* **133**(3), 595–602 (2011).
238. H. M. Chen et al., "Plasmon inducing effects for enhanced photoelectrochemical water splitting: x-ray absorption approach to electronic structures," *ACS Nano* **6**(8), 7362–7372 (2012).
239. P. A. DeSario et al., "Plasmonic enhancement of visible-light water splitting with Au-TiO_2 composite aerogels," *Nanoscale* **5**(5), 8073–8083 (2013).
240. X. Zhang et al., "Coupling surface plasmon resonance of gold nanoparticles with slow-photon-effect of TiO_2 photonic crystals for synergistically enhanced photoelectrochemical water splitting," *Energy Environ. Sci.* **7**(4), 1409–1419 (2014).
241. H. Xie et al., "Facile fabrication of 3D-ordered macroporous nanocrystalline iron oxide films with highly efficient visible light induced photocatalytic activity," *J. Phys. Chem. C* **114**(21), 9706–9712 (2010).
242. M. Sadakane et al., "Preparation of 3-D ordered macroporous tungsten oxides and nanocrystalline particulate tungsten oxides using a colloidal crystal template method, and their structural characterization and application as photocatalysts under visible light irradiation," *J. Mater. Chem.* **20**(9), 1811–1818 (2010).
243. X. Chen et al., "Enhanced incident photon-to-electron conversion efficiency of tungsten trioxide photoanodes based on 3D-photonic crystal design," *ACS Nano* **5**(6), 4310–4318 (2011).
244. L. Zhang et al., "Bi_2WO_6 inverse opals: facile fabrication and efficient visible-light-driven photocatalytic and photoelectrochemical water-splitting activity," *Small* **7**(19), 2714–2720 (2011).
245. L. Zhang et al., "Plasmonic enhancement in $BiVO_4$ for efficient water splitting," *Small* **10**(19), 3970–3978 (2014).
246. H. Liu et al., "Hydrogen evolution *via* sunlight water splitting on an artificial butterfly wing architecture," *Phys. Chem. Chem. Phys.* **13**(23), 10872–10876 (2011).
247. H. Zhou et al., "Artificial inorganic leafs for efficient photochemical hydrogen production inspired by natural photosynthesis," *Adv. Mater.* **22**(9), 951–956 (2010).
248. H. Mousazadeh et al., "A review of principle and sun-tracking methods for maximizing solar systems output," *Renewable Sustainable Energy Rev.* **13**, 1800–1818 (2009).

Downloaded From: http://photonicsforenergy.spiedigitallibrary.org/ on 01/26/2016 Terms of Use: http://spiedigitallibrary.org/ss/TermsOfUse.aspx

249. C.-Y. Lee et al., "Sun tracking systems: a review," *Sensors* **9**, 3875–3890 (2009).
250. S. S. Kalogirou, *Solar Energy Engineering. Processes and Systems*, Academic Press, Amsterdam (2009).
251. F. Duerr, Y. Meuret, and H. Thienpont, "Tailored free-form optics with movement to integrate tracking in concentrating photovoltaics," *Opt. Express* **21**(103), A401–A411 (2013).
252. J. F. Song et al., "Configuration of daylighting system via fibers an experiments of concentrated sunlight transmission," in *Proc. of the World Renewable Energy Congress*, 8–13 May 2011, Linköping, Sweden, pp. 3781–3788 (2011).
253. G. M. Tina, F. Arcidiacono, and A. Gagliano, "Intelligent sun-tracking system based on multiple photodiode sensors for maximisation of photovoltaic energy production," *Math. Comput. Simul.* **91**, 16–28 (2013).
254. T. K. Kragas, B. A. Williams, and G. A. Myers, "The optic oil field: deployment and application of permanent in-well fiber optic sensing systems for production and reservoir monitoring," Paper No. SPE-71529-MS, *Soc. Petrol. Eng.* (2001).
255. K. Ferguson, "Fiber optic sensors in the oil industry," http://large.stanford.edu/courses/2011/ph240/ferguson1/ (2014).
256. G. Brown, "Downhole temperatures from optical fiber," *Oil Field Rev.* **20**, 34 (2009).
257. S. J. Mihailov, "Fiber Bragg grating sensors for harsh environments," *Sensors* **12**, 1898–1918 (2012).
258. Weatherford, "Downhole Fiber Optic Distributed Temperature Sensing System," (2002), http://www.ipt.ntnu.no/~asheim/ovinger/Golan/Fiber%20Optic.pdf (17 August 2015).
259. P. J. M. Clive, Windpower 2.0: technology rises to the challenge, *Environ. Res. Web* http://environmentalresearchweb.org/cws/article/opinion/36322 (17 August 2014).
260. A. K. Scholbrock et al., "Field testing LIDAR based feed-forward controls on the NREL controls advanced research turbine," in *51st AIAA Aerospace Sciences Meeting*, Grapevine, Texas (2013), http://www.nrel.gov/docs/fy13osti/57339.pdf.
261. J. G. Fleming et al., "All-metallic three-dimensional photonic crystals with a large infrared bandgap," *Nature* **417**, 52–55 (2002).
262. http://apps1.eere.energy.gov/buildings/publications/pdfs/ssl/ssl_mfg_roadmap_aug2014.pdf.
263. M. R. Krames et al., "High-power truncated-inverted-pyramid (AlxGa1-x)(0.5)In0.5P/GaP light-emitting diodes exhibiting > 50% external quantum efficiency," *Appl. Phys. Lett.* **75**, 2365–2367 (1999).
264. H. Amano et al., "Metalorganic vapor-phase epitaxial growth of a high quality GaN film using an AlN buffer layer," *Appl. Phys. Lett.* **48**, 353 (1986).
265. S. Nakamura, T. Mukai, and M. Senoh, "High-power GaN P-N junction blue-light-emitting diodes," *Jpn. J. Appl. Phys.* **30**, L1998–L2001 (1991).
266. I. Akasaki et al., "GaN-based UV /blue light emitting devices," *Inst. Phys. Conf. Ser.* **129**, 851 (1992).
267. S. Nakamura et al., "P-GaN/N-InGaN/N-GaN double-heterostructure blue-light-emitting diodes," *Jpn. J. Appl. Phys.* **32**, L8 (1993).
268. J. Nelson et al., "Compositional dependence of the luminescence of $In_{0.49}(AlyGa_{1-y})_{0.51}P$ alloys near the direct-indirect band-gap crossover," *Phys. Rev. B* **53**, 15893 (1996).
269. P. M. Smowton and P. Blood, *IEEE J. Sel. Top. Quantum Electron.* **3**, 491 (1997).
270. D. Bour et al., "Drift leakage current in AlGaInP quantum-well lasers," *IEEE J. Quantum Electron.* **29**, 1337 (1993).
271. N. Tansu and L. J. Mawst, "Current injection efficiency of 1300-nm InGaAsN quantum-well lasers," *J. Appl. Phys.* **97**(5), 054502 (2005).
272. J. I. Pankove et al., "GaN blue light-emitting diodes," *J. Lumin.* **5**, 84 (1972).
273. O. H. Nam et al., "Lateral epitaxy of low defect density GaN layers via organometallic vapor phase epitaxy," *Appl. Phys. Lett.* **71**, 2638–2640 (1997).
274. S. Nakamura et al., "Room-temperature continuous-wave operation of InGaN multi-quantum-well structure laser diodes," *Appl. Phys. Lett.* **69**, 4056 (1996).
275. D. Feezell et al., "Semipolar $(20\overline{2}1)$ InGaN/GaN light-emitting diodes for high-efficiency solid-state lighting," *J. Disp. Technol.* **9**, 190–198 (2013).
276. R. A. Arif et al., "Polarization engineering via staggered InGaN quantum wells for radiative efficiency enhancement of light emitting diodes," *Appl. Phys. Lett.* **91**, 091110 (2007).

Downloaded From: http://photonicsforenergy.spiedigitallibrary.org/ on 01/26/2016 Terms of Use: http://spiedigitallibrary.org/ss/TermsOfUse.aspx

277. H. Zhao et al., "Approaches for high internal quantum efficiency green InGaN light-emitting diodes with large overlap quantum wells," *Opt. Express* **19**(S4), A991–A1007 (2011).
278. T. W. Yeh et al., "InGaN/GaN multiple quantum wells grown on nonpolar facets of vertical GaN nanorod arrays," *Nano Lett.* **12**, 3257–3262 (2012).
279. Cree press release, "Cree first to break 300 lumens per watt barrier," http://www.cree.com/News-and-Events/Cree-News/Press-Releases/2014/March/300LPW-LED-barrier (22 August 2015).
280. M. H. Crawford, "LEDs for solid-state lighting: performance challenges and recent advances," *IEEE J. Sel. Top. Quantum Electron.* **15**, 1028–1040 (2009).
281. N. Tansu et al., "III-nitride photonics," *IEEE Photonics J.* **2**(2), 241–248 (2010).
282. Y. K. Ee et al., "Metalorganic vapor phase epitaxy of III-nitride light-emitting diodes on nano-patterned AGOG sapphire substrate by abbreviated growth mode," *IEEE J. Sel. Top. Quantum Electron.* **15**(4), 1066–1072 (2009).
283. Y. K. Ee et al., "Abbreviated MOVPE nucleation of III-nitride light-emitting diodes on nano-patterned sapphire," *J. Cryst. Growth* **312**(8), 1311–1315 (2010).
284. Y. Li et al., "Defect-reduced green GaInN/GaN light-emitting diode on nanopatterned sapphire," *Appl. Phys. Lett.* **98**(15), 151102 (2011).
285. A. Alizadeh et al., "Templated wide band-gap nanostructures," *J. Appl. Phys.* **95**(12), 8199 (2004).
286. Toshiba Machine, "Micro-pattern imprinting machine ST series," http://www.toshiba-machine.co.jp/en/product/nano/lineup/st/st50s.html (22 August 2015).
287. H. P. Zhao, G. Y. Liu, and N. Tansu, "Analysis of InGaN-delta-InN quantum wells for light-emitting diodes," *Appl. Phys. Lett.* **97**, 131114 (2010).
288. T. Frost et al., "InGaN/GaN quantum dot red laser," *IEEE J. Quantum Electron.* **49**, 923–931 (2013).
289. J. Zhang and N. Tansu, "Optical gain and laser characteristics of InGaN quantum wells on ternary InGaN substrates," *IEEE Photonics J.* **5**(2), 2600111 (2013).
290. M. Funato et al., "Monolithic Polychromatic Light-Emitting Diodes Based on InGaN Microfacet Quantum Wells toward Tailor-Made Solid-State Lighting," *Appl. Phys. Express* **1**, 011106 (2008).
291. W. W. Chow et al., "Internal efficiency of InGaN light-emitting diodes: Beyond a quasiequilibrium model," *Appl. Phys. Lett.* **97**, 121105 (2010).
292. S. Choi et al., "Improvement of peak quantum efficiency and efficiency droop in III-nitride visible light-emitting diodes with an InAlN electron-blocking layer," *Appl. Phys. Lett.* **96**(22), 221105 (2010).
293. H. J. Kim et al., "Improvement of quantum efficiency by employing active-layer-friendly lattice-matched InAlN electron blocking layer in green light-emitting diodes," *Appl. Phys. Lett.* **96**(10), 101102 (2010).
294. G. Y. Liu et al., "Efficiency-droop suppression by using large-bandgap AlGaInN thin barrier layers in InGaN quantum wells light-emitting diodes," *IEEE Photonics J.* **5**(2), 2201011 (2013).
295. H. P. Zhao et al., "Analysis of internal quantum efficiency and current injection efficiency in nitride light-emitting diodes," *J. Disp. Technol.* **9**(4), 212–225 (2013).
296. K. T. Delaney, P. Rinke, and C. G. Van de Walle, "Auger recombination rates in nitrides from first principles," *Appl. Phys. Lett.* **94**(19), 191109 (2009).
297. J. Iveland et al., "Direct measurement of Auger electrons emitted from a semiconductor light-emitting diode under electrical injection: identification of the dominant mechanism for efficiency droop," *Phys. Rev. Lett.* **110**(17), 177406 (2013).
298. C. K. Tan et al., "First-principle electronic properties of dilute-As GaNAs alloy for visible light emitters," *J. Disp. Technol.* **9**(4), 272–279 (2013); J. Iveland*Phys. Rev. Lett.* **110**, 177406 (2013).
299. S. Pimputkar et al., "Improved growth rates and purity of basic ammonothermal GaN," *J. Cryst. Growth* **403**, 7–17 (2014).
300. S. E. Brinkley et al., "Robust thermal performance of Sr2Si5N8:Eu2+: an efficient red emitting phosphor for light emitting diode based white lighting," *Appl. Phys. Lett.* **99**, 241106 (2011).

Downloaded From: http://photonicsforenergy.spiedigitallibrary.org/ on 01/26/2016 Terms of Use: http://spiedigitallibrary.org/ss/TermsOfUse.aspx

301. J. J. Wierer, A. David, and M. M. Megens, "BIII-nitride photonic-crystal light-emitting diodes with high extraction efficiency," *Nat. Photonics* **3**(3), 163–169 (2009).
302. X. H. Li et al., "Light extraction efficiency and radiation patterns of III-nitride light-emitting diodes with colloidal microlens arrays with various aspect ratios," *IEEE Photonics J.* **3**(3), 489–499 (2011).
303. J. Jewell et al., "Double embedded photonic crystals for extraction of guided light in light-emitting diodes," *Appl. Phys. Lett.* **100**, 171105 (2012).
304. J. Y. Tsao et al., "Toward smart and ultra-efficient solid-state lighting," *Adv. Opt. Mater.* **2**(9), 809–836 (2014).
305. C. W. Tang and S. A. Vanslyke, "Organic electroluminescent diodes," *Appl. Phys. Lett.* **51**, 12 (1987).
306. J. Kido, M. Kimura, and K. Nagai, "Multilayer white light-emitting organic electroluminescent device," *Science* **267**(5202), 1332–1334 (1995).
307. M. A. Baldo et al., "Excitonic singlet-triplet ratio in a semiconducting organic thin film," *Phys. Rev. B* **60**(20), 14422–14428 (1999).
308. T. Fleetham and J. Li, "Recent advances in white organic light-emitting diodes employing a single-emissive material," *J. Photonics Energy* **4**(1), 040991 (2014).
309. G. L. Ingram and Z.-H. Lu, "Design principles for highly efficient organic light-emitting diodes," *J. Photonics Energy* **4**(1), 040993 (2014).
310. LG Chemical, "OLED light," http://www.lgchem.com/global/green-energy/oled-lighting (22 August 2015).
311. Konica Minolta, "Flexible OLED lighting," http://www.konicaminolta.com/oled/products/index.html (22 August 2015).
312. W. Cao et al., "Transparent electrodes for organic optoelectronics devices: a review," *J. Photonics Energy* **4**(1), 040990 (2014).
313. L. Ding et al., "A novel intermediate connector with improved charge generation and separation for large-area tandem white organic lighting devices," *J. Mater. Chem. C* **2**, 48 (2014).
314. R. A. Street, "Luminescence and recombination in hydrogenated amorphous silicon," *Adv. Phys.* **30**, 593–676 (1981).
315. D. E. Carlson et al., "Hydrogenated amorphous silicon—a solar cell material," *Thin Solid Film* **45**, 43–46 (1977).
316. M. C. Abdulrida and J. Allison, "Influence of hydrogen on the performance of magnetron-sputtered amorphous hydrogenated silicon field-effect transistors," *Appl. Phys. Lett.* **43**, 768–770 (1983).
317. N. C. Greenham, R. H. Friend, and D. D. Bradley, "Angular dependence of the emission from a conjugated polymer light-emitting diode: implications for efficiency calculations," *Adv. Mater.* **6**, 491–494 (1994).
318. P.A. Hobson et al., "Surface plasmon mediated emission from organic light-emitting diodes," *Adv. Mater.* **14**, 1393–1396 (2002).
319. S. Moller and S. R. Forrest, "Improved light out-coupling in organic light emitting diodes employing ordered microlens arrays," *J. Appl. Phys.* **91**, 3324–3327 (2002).
320. S. M. Chen and H. S. Kwok, "Light extraction from organic light-emitting diodes for lighting applications by sand-blasting substrates," *Opt. Express* **18**, 37–42 (2010).
321. Y. H. Cheng et al., "Enhanced light outcoupling in a thin film by texturing meshed surfaces," *Appl. Phys. Lett.* **90**, 091102 (2007).
322. B. J. Matterson et al., "Increased efficiency and controlled light output from a microstructured light-emitting diode," *Adv. Mater.* **13**, 123 (2001).
323. Y. R. Do et al., "Enhanced light extraction from organic light-emitting diodes with 2D SiO_2/SiN_x photonic crystals," *Adv. Mater.* **15**, 1214 (2003).
324. Y. Sun and S. R. Forrest, "Enhanced light out-coupling of organic light-emitting devices using embedded low-index grids," *Nat. Photonics* **2**, 483–487 (2008).
325. W. H. Koo et al., "Light extraction from organic light-emitting diodes enhanced by spontaneously formed buckles," *Nat. Photonics* **4**, 222–226 (2010).
326. S. Mladenovski et al., "Exceptionally efficient organic light emitting devices using high refractive index substrates," *Opt. Express* **17**, 7562–7570 (2009).

Downloaded From: http://photonicsforenergy.spiedigitallibrary.org/ on 01/26/2016 Terms of Use: http://spiedigitallibrary.org/ss/TermsOfUse.aspx

327. J. B. Kim et al., "Highly enhanced light extraction from surface plasmonic loss minimized organic light-emitting diodes," *Adv. Mater.* **25**, 3571–3577 (2013).
328. C. J. Yates et al., "Surface plasmon-polariton mediated emission from phosphorescent dendrimer light-emitting diodes," *Appl. Phys. Lett.* **88**, 161105 (2006).
329. J. J. Greffet, "Nanoantennas for light emission," *Science* **308**, 1561 (2005).
330. J. R. Lakowicz, "Plasmonics in biology and plasmon-controlled fluorescence," *Plasmonics* **1**, 5–33 (2006).
331. P. Bharadwaj and L. Novotny, "Spectral dependence of single molecule fluorescence enhancement," *Opt. Express* **15**, 14266–14274 (2007).
332. T. H. Taminiau, F. D. Stefani, and N. F. van Hulst, "Single emitters coupled to plasmonic nano-antennas: angular emission and collection efficiency," *New J. Phys.* **10**, 105005 (2008).
333. J. Vuckovic, M. Loncar, and A. Scherer, "Surface plasmon enhanced light-emitting diode," *IEEE J. Quantum Electron.* **36**, 1131–1144 (2000).
334. A. Neogi et al., "Enhancement of spontaneous recombination rate in a quantum well by resonant surface plasmon coupling," *Phys. Rev. B* **66**, 153305 (2002).
335. K. Okamoto et al., "Surface-plasmon-enhanced light emitters based on InGaN quantum wells," *Nat. Mater.* **3**, 601–605 (2004).
336. S. McDaniel and S. Blair, "Increased OLED radiative efficiency using a directive optical antenna," *Opt. Express* **18**, 17477–17483 (2010).
337. C. Foss, "Beacon," in *The Oxford Dictionary of Byzantium*, A. Kazhdan, pp. 273–274, Oxford University Press, Oxford, United Kingdom (1991).
338. A. G. Bell and S. Tainter, "Selenium and the photophone," *Nature* **22**, 500–503 (1880).
339. M. Asghari and A. V. Krishnamoorthy, *Nat. Photonics* **5**, 268 (2011).
340. G. P. Agrawal, *Fiber-Optic Communication Systems*, John Wiley & Sons, New York (2002).
341. T. Toma et al., "High speed optical home network using graded index plastic optical fibers for a smart house," *ACSIJ Adv. Comput. Sci. Int. J.* **2**(5–6), 141–149 (2013).
342. D. A. B. Miller, "Device requirements for optical interconnects to silicon chips," *Proc. IEEE* **97**, 1166–1185 (2009).
343. K. Schmidtke et al., "960 Gb/s optical backplane ecosystem using embedded polymer waveguides and demonstration in a 12G SAS storage array," *IEEE J. Lightwave Technol.* **31**, 3970–3974 (2013).
344. Tech Watch, "Silicon Photonics," http://www.jazdtech.com/techdirect/leaf/IT-Hardware/Components/Silicon-Photonics.htm (22 August 2015).
345. J. F. Buckwalter et al., "A Monolithic 25-Gb/s Transceiver With Photonic Ring Modulators and Ge Detectors in a 130-nm CMOS SOI Process," *IEEE J. Solid State Circuits* **47**, 1309–1322 (2012).
346. D. Liang and J. E. Bowers, "Recent progress in lasers on silicon," *Nat. Photonics* **4**, 511–517 (2010).
347. R. Tucker, "Green optical communications—Part I: Energy limitations in transport," *IEEE J. Sel. Top. Quantum Electron.* **17**, 245–260 (2011).
348. R. Tucker, "Green optical communications—Part II: Energy limitations in networks," *IEEE J. Sel. Top. Quantum Electron.* **17**, 261–274 (2011).
349. K. Nozaki et al., "Sub-femtojoule all-optical switching using a photonic-crystal nanocavity," *Nat. Photonics* **4**, 477 (2010).

Zakya H. Kafafi received her PhD in chemistry from Rice University. She started her career as an assistant professor in Egypt before moving back to the United States, where she held several posts in academia: at the Naval Research Laboratory (NRL), where she established an interdisciplinary research team in Organic Optoelectronics, and at National Science Foundation as the director of the Division of Materials Research. She is a member of ACS, Sigma Xi, and is a fellow of AAAS, MRS, OSA, and SPIE.

Ana F. Nogueira received her PhD in inorganic chemistry from the University of Campinas (UNICAMP) in 2001. After a postdoctoral position in the group of James R. Durrant at the Imperial College, London, where she investigated organic and hybrid solar cells, she was appointed on the faculty of UNICAMP, where she currently holds the position of associate

Downloaded From: http://photonicsforenergy.spiedigitallibrary.org/ on 01/26/2016 Terms of Use: http://spiedigitallibrary.org/ss/TermsOfUse.aspx

professor. She is also the coordinator of the Laboratory of Nanotechnology and Solar Energy in Brazil.

Raúl J. Martín-Palma is a professor of physics at the Universidad Autónoma de Madrid and adjunct professor at the Pennsylvania State University's Department of Materials Science and Engineering. He received his MS and PhD degrees in physics in 1995 and 2000, respectively, from the Universidad Autónoma de Madrid. He was a postdoctoral fellow at the New Jersey Institute of Technology and a visiting professor at Pennsylvania State University. He received young scientists' awards from MRS and the European MRS for his research on nanostructured materials.

Deirdre M. O'Carroll is an assistant professor in the Department of Materials Science and Engineering at Rutgers University. Her research interests are focused on light generating and light harvesting processes in organic polymer semiconductors and plasmonic nanostructures. Her research has a number of end uses such as light management in thin-film organic optoelectronics, optically active electrodes, nanoscale optical devices, and environmentally friendly electronics and photonics. She received her PhD in microelectronic engineering from the University College Cork in Ireland.

Jeremy J. Pietron received his PhD in analytical chemistry from the University of North Carolina at Chapel Hill in 1998. After completing a National Research Council postdoctoral fellowship at the NRL in Washington DC from 1999 to 2002, he joined the laboratory as a full-time staff scientist in 2003. His primary research interests are nanostructured materials, electrocatalysis, plasmonic nanomaterials, heterogeneous catalysis, and solar fuels photocatalysis.

Ifor D. W. Samuel is a professor of physics and director of the Organic Semiconductor Centre at the University of St Andrews. He received his MA and PhD degrees from the University of Cambridge and performed postdoctoral work at Centre National d'Etudes des Télécommunications of France Telecom in Paris. His current work focuses on the photophysics of organic semiconductor materials and devices. He is a fellow of the Royal Society of Edinburgh, the Institute of Physics, the Royal Society of Chemistry, and SPIE.

Franky So received his PhD in electrical engineering from the University of Southern California. From 1993 to 2005, he was with Motorola and OSRAM before he moved to the University of Florida as a professor in the Materials Science and Engineering (MSE) Department. In 2015, he joined North Carolina State University as the Walter and Ida Freeman distinguished professor in the MSE Department. His research interest is in the area of organic electronics.

Nelson Tansu is the Daniel E. '39 and Patricia M. Smith endowed chair professor in photonics and nanoelectronics at Lehigh University. His research interests lie in the physics of semiconductor optoelectronics materials and devices, low-dimensional semiconductor nanostructures, and III-nitride and III–V–nitride semiconductor optoelectronics devices on GaAs, InP, and GaN substrates. He received his BS and PhD degrees in electrical engineering/applied physics from the University of Wisconsin-Madison in 1998 and 2003, respectively.

Loucas Tsakalakos is the manager of the Photonics Laboratory at General Electric–Global Research in New York. He received his BS degree from Rutgers University in 1995, and his MS and PhD degrees in materials science and engineering from U.C. Berkeley in 1998 and 2000, respectively. He has worked on sensors, lighting, nanotechnology, and photovoltaics. He is a member of Tau Beta Pi (The National Engineering Honor Society), author/co-author of over 30 publications, and holds 14 U.S. patents.

Downloaded From: http://photonicsforenergy.spiedigitallibrary.org/ on 01/26/2016 Terms of Use: http://spiedigitallibrary.org/ss/TermsOfUse.aspx